Fluid-rich damage zone of an ancient out-of-sequence thrust, Kodiak Islands, Alaska

Christen D. Rowe,[1,2] Francesca Meneghini,[1,3] and J. Casey Moore[1]

Received 1 March 2007; revised 5 October 2008; accepted 14 November 2008; published 18 February 2009.

[1] The Uganik Thrust is a fossil out-of-sequence thrust fault which was active over a period of ~3 Ma during the early Tertiary until activity ceased with the subduction of the Kula-Farallon spreading ridge at ~57 Ma. During this period the fault experienced at least ~1 km of throw and developed a strongly asymmetric damage zone. The brittle damage zone in the footwall of the fault acted as a conduit for fluid advection during the active faulting. A similar asymmetrical footwall damage zone has been interpreted as a fluid conduit at the Nobeoka Thrust, Shimanto Belt, SW Japan. Thermal indicators in the uppermost footwall give similar maximum paleotemperatures to those in the hanging wall (~280°C), while previous work elsewhere in the footwall formation suggests maximum burial temperatures of ~240°C. In this case, similar to the Irish Canyon thrust in the Franciscan accretionary complex, the location of the thermal anomaly is spatially offset from the structural fault which caused it owing to thermal overprinting in the vicinity of the fault. **Citation:** Rowe, C. D., F. Meneghini, and J. C. Moore (2009), Fluid-rich damage zone of an ancient out-of-sequence thrust, Kodiak Islands, Alaska, *Tectonics*, *28*, TC1006, doi:10.1029/2007TC002126.

1. Introduction

[2] Thrust faults in the out-of-sequence geometry (out-of-sequence thrust faults, OOSTs) are increasingly recognized as an important part of the plate boundary fault system in many subduction zone settings. The term "OOST" describes splay faults which form in the hanging wall of a preexisting basal thrust to which they are listric [*Cummins et al.*, 2001; *Davis and Reynolds*, 1996]. They are "out-of-sequence" in the sense of having formed behind the trace of the basal thrust, rather than forming sequentially in the direction of hanging wall propagation.

[3] Very large earthquakes which nucleate on the décollement thrust may propagate upward along an OOST [*Clarke et al.*, 1992; *Cummins et al.*, 2001; *Plafker*, 1972]. OOST are more steeply dipping at the seafloor than the décollement thrust, and can cause vertical motion of the seafloor that may increase the risk of tsunami generation [*Cummins et al.*, 2001; *Park et al.*, 2000]. Ruptures of this style have been invoked to explain the extraordinary tsunamis caused by some earthquakes such as Alaska 1964 [*Plafker*, 1972], the peculiarly large runup in the Banda Aceh region during the December 2004 tsunami [*Lay et al.*, 2005] and the 1946 Nankai earthquake [*Park et al.*, 2000].

[4] Seafloor venting of fresh water, methane, and CO_2 has been associated with the surface traces of active OOST [*Carson et al.*, 2003; *Park et al.*, 2000; *Riedel et al.*, 2002] and the source of these fluids may be dewatering subducting sediment, via intersection with an active décollement [*Vrolijk*, 1987b]. Recent observations of very low-frequency earthquakes in the Nankai accretionary prism are consistent with reverse motion on faults within the prism, although they are not well located [*Ito and Obara*, 2006a, 2006b]. The low velocity and low stress drops calculated for these events may be attributable to water present along the fault [*Ito and Obara*, 2006a, 2006b]. Seismic reflection surveys in modern subduction environments have revealed that the "bottom-simulating" or gas hydrate reflector (BSR) along out-of-sequence thrusts is locally elevated, providing evidence for the advection of warm fluids along active faults [*Zwart et al.*, 1996]. Both décollement and out-of-sequence thrusts provide high-permeability pathways for significant fluid escape from the décollement interface. Therefore, thrusts in this geometry must be considered part of the plate boundary fault system, and a discussion of subduction zone seismicity is incomplete without an understanding of these structures. Most OOST crop out on the seafloor and are not available for direct geologic study, but fieldwork in ancient accretionary complexes has the potential to investigate OOST in the rock record.

[5] Low-temperature metasedimentary terranes present difficult problems to geologists because of disequilibrium geochemistry and incomplete metamorphism. Accretionary complexes present the additional complications of substantial deformation during the process of accretion, resulting in an overprinted structural record through deposition, burial, subduction, underplating, wedge shortening, and exhumation. Pristine examples of subduction-related structures are rare and rarely recognized. However, several studies have succeeded in differentiating OOST from other thrust faults in fossil accretionary wedges, mostly on the basis of an additional phase of shortening/deformation along the fault,

[1]Earth and Planetary Sciences, University of California, Santa Cruz, California, USA.
[2]Now at Department of Geological Sciences, University of Cape Town, Rondebosch, South Africa.
[3]Now at Dipartimento di Scienze della Terra, Università di Pisa, Pisa, Italy.

0278-7407/09/2007TC002126$12.00

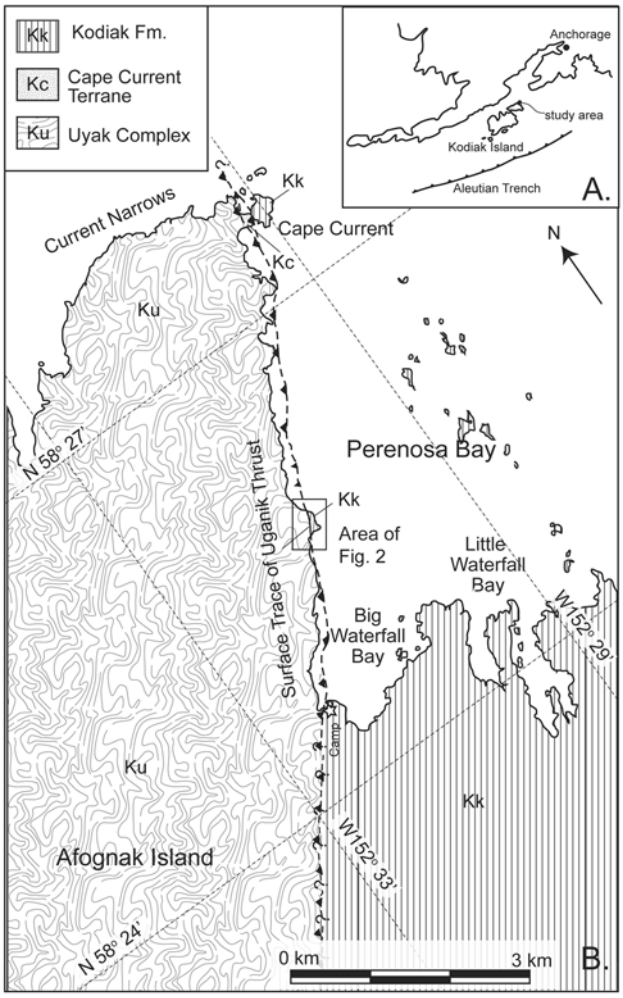

Figure 1. Study location. (a) Inset map showing location of Kodiak Archipelago, Gulf of Alaska. (b) Study area at Big Waterfall Bay, Afognak Island. Base map modified from Google Earth imagery; geology modified from *Connelly* [1976].

or evidence of postthermal peak offset [*DiTullio and Byrne*, 1990; *Kondo et al.*, 2005; *Kusaba et al.*, 2006; *Ohmori et al.*, 1997; *Underwood and Laughland*, 2001].

[6] In the context of the Coulomb model accretionary wedge, OOST play an important role in maintaining critical taper by thickening the wedge during exhumation of the hanging wall [*Kimura et al.*, 2007; *Shelton et al.*, 1996; *Underwood et al.*, 1996]. Out-of-sequence thrusts dissect and displace preexisting thermal structure of the wedge. As a result, OOST and other postthermal peak thrusts have been identified in the ancient record by thermal gaps across the fault [*Kondo et al.*, 2005; *Kusaba et al.*, 2006; *Ohmori et al.*, 1997; *Shelton et al.*, 1996; *Tsuji et al.*, 2006; *Underwood et al.*, 1993a, 1996; *Underwood and Laughland*, 2001].

[7] At relatively low pressures and temperatures in the shallow toe of an accretionary wedge, commonly used geothermobarometers give relatively low resolution and some techniques may be affected by other factors such as duration of burial and shear in sediments. In the absence of a clearly measurable thermal gap, OOST can be identified by geometry and crosscutting relationships relative to subduction-related deformation structures in the wall rocks.

[8] This study reports a detailed analysis of the structural, thermal, and fluid flow history of the Uganik Thrust, a terrane-bounding fault from the Kodiak accretionary complex. Documentation of two discrete periods of faulting history: a multiphase evolution during subduction, cross cut by slightly more steeply dipping thrust fabrics associated with veins of a distinct fluid inclusion population, motivates our interpretation that the Uganik Thrust was most recently active as an OOST. The Uganik Thrust provides insight on the scale, style, and geometry of out-of-sequence thrusts, and demonstrates localization of fluid flow and associated deformation.

2. Geologic Setting

2.1. Kodiak Accretionary Complex

[9] The Kodiak accretionary complex (and equivalents) make up the modern Aleutian fore arc in south central Alaska (Chugach and Prince William terranes of *Plafker et al.* [1994]) (Figure 1). The complex is composed of a series of accreted terranes of marine sediments and basalt. Each of these terranes is distinguished from its neighbors by depositional age, lithologic assemblage, and metamorphic grade [*Byrne*, 1982; *Connelly*, 1978; *Moore*, 1969; *Moore and Allwardt*, 1980; *Roeske*, 1986; *Sample and Fisher*, 1986]. The boundaries between these terranes likely originated as thrust faults although some show evidence of reactivation [*Roeske et al.*, 1989]. The trench-parallel structure of the Kodiak accretionary complex with increasing metamorphic grade and age away from the trench is mirrored in the megascale structure of other accretionary complexes (e.g., Franciscan Complex, California, Shimanto Belt, Japan, and Sesia Complex, the Alps [*Connelly*, 1978; *Ernst*, 1971; *Taira et al.*, 1988]) and reflects punctuated accretion of oceanic material in a long-lived subduction system.

2.2. Uganik Thrust

[10] The Uganik Thrust (Figures 1 and 2) juxtaposes the Uyak Complex over the Waterfall Bay mélange, a zone of stratal disruption at the structural top of the Kodiak Formation [*Fisher and Byrne*, 1987; *Moore*, 1978]. Along strike, the Uganik Thrust is correlated with the Chugach Bay Fault in the Kenai Mountains [*Kusky et al.*, 1993; *Magoon et al.*, 1976] and the Eagle River Fault near Anchorage [*Clarke and Samuel*, 1972]. Previous workers described the Uganik Thrust and determined its association with NW directed subduction during the late Cretaceous [*Connelly*, 1976, 1978; *Moore*, 1978].

[11] The Uganik Thrust dips more steeply than structural fabrics in the footwall. Fault-related deformation associated with the Uganik Thrust is characterized by cataclasis, grain boundary migration and quartz cementation while earlier, subduction-related deformational fabrics are characterized

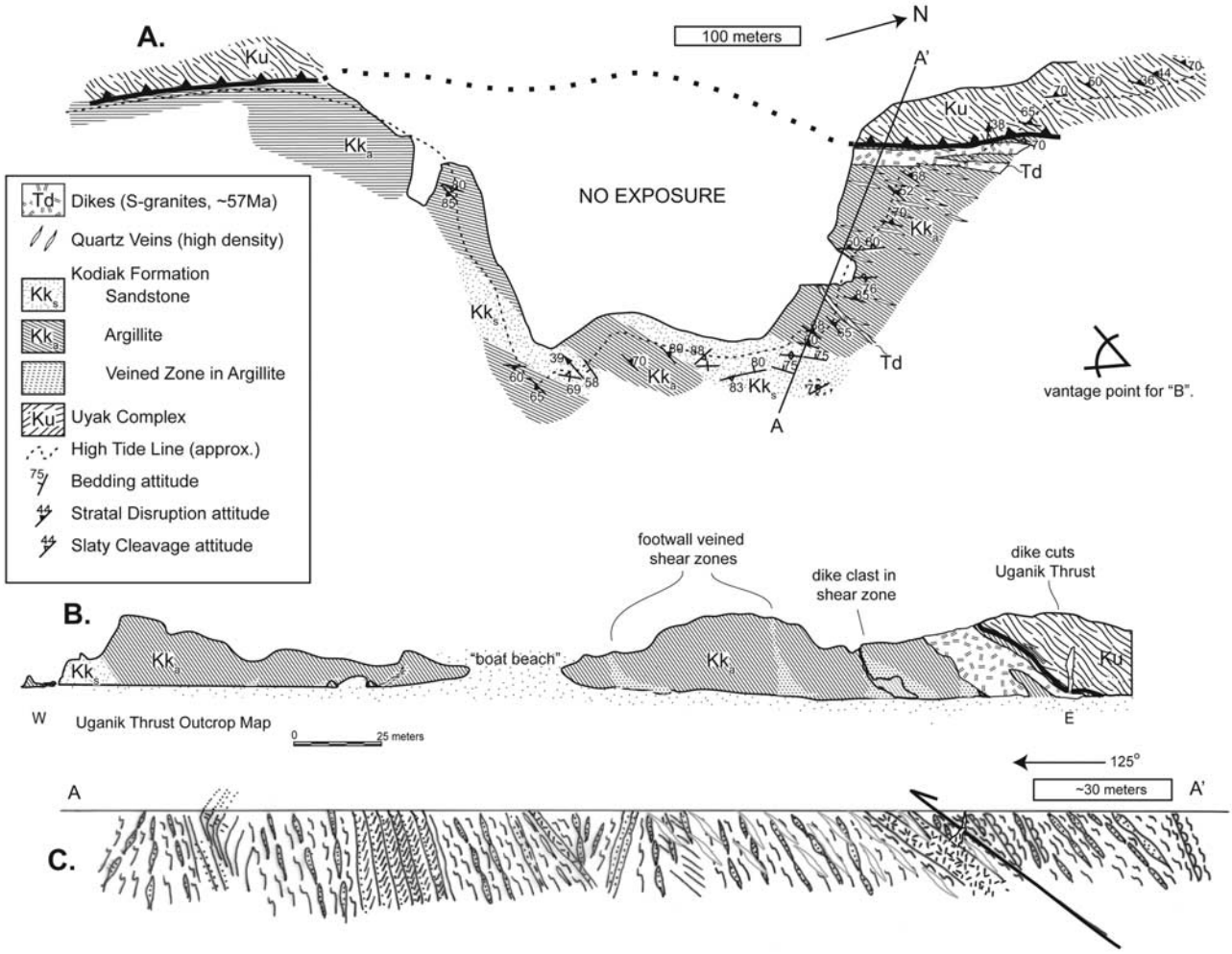

Figure 2. (a) Small-scale map of studied locality, including vein distribution and sandy versus argillitic lithologies within the Kodiak Formation. Vantage point is shown for offshore view of outcrop (shown in Figure 2b). (b) Panoramic view of outcrop (pseudosection shown is approximately parallel to dip azimuth of fault and local fabrics). (c) Cross section A-A″ showing folded/faulted structure in the Kodiak Formation (Waterfall Bay mélange) and Uyak Complex, both crosscut by the Uganik Thrust.

by pressure solution cleavage and calcite or quartz-filled extensional fractures, suggesting flattening and pressure solution creep. We therefore interpret the Uganik Thrust as an out-of-sequence thrust fault (OOST), which postdates and crosscuts earlier, décollement-related deformation in the uppermost Kodiak Formation (Waterfall Bay mélange).

2.3. Uyak Complex (Hanging Wall)

[12] The Uyak Complex is a formation-scale mélange dominated by black argillite interbedded with gray chert, with lesser proportions of basalt (pillow and subaqueous hyaloclastite), red chert, and graywacke, and rare ultramafic blocks [*Connelly*, 1978]. It is described in detail along strike in the Kenai Mountains where it is known as the McHugh Complex [*Bradley and Kusky*, 1992; *Kusky and Bradley*, 1999]. Microfossil ages cluster from Tithonian to Valanginian (151–135 Ma), but range from Paleozoic to middle-Early Cretaceous [*Connelly*, 1978; *Plafker and Nokleberg*, 1987]. The upper limit of radiolarian ages suggests accretion occurred at ~100 Ma [*Plafker and Nokleberg*, 1987]. Mafic lithologies and some graywackes contain abundant prehnite and pumpellyite [*Connelly*, 1978]. The Uyak Complex is interpreted as a macroscopic mélange formed during NW directed subduction of oceanic crust with a thin sediment covering [*Byrne*, 1985; *Kusky and Bradley*, 1999; *Moore*, 1978].

[13] The Uyak Complex observed at Big Waterfall Bay is composed of black argillite, light green basaltic hyaloclastite, and gray chert (Figure 3a). Chert, greenstone and graywacke occur as large blocks (meter to 10 s meters) with a scaly argillite matrix. The argillite is metamorphosed to fine grained chlorite, albite and quartz and occasional pyrite. Pumpellyite is common in mafic and mixed lithologies.

2.4. Kodiak Formation and the Waterfall Bay Mélange (Footwall)

[14] The Kodiak Formation is a structural stack of variably coherent sequences of deep water turbidites, quartzitic to lithic graywacke sandstones, rare conglomerates and pebbly mudstones. It was deposited rapidly into an actively subducting trench during the Maastrictian (latest Cretaceous) [*McCann and Pickerill*, 1988; *Moore*, 1978]. Fluid inclusion measurements by previous workers suggest that

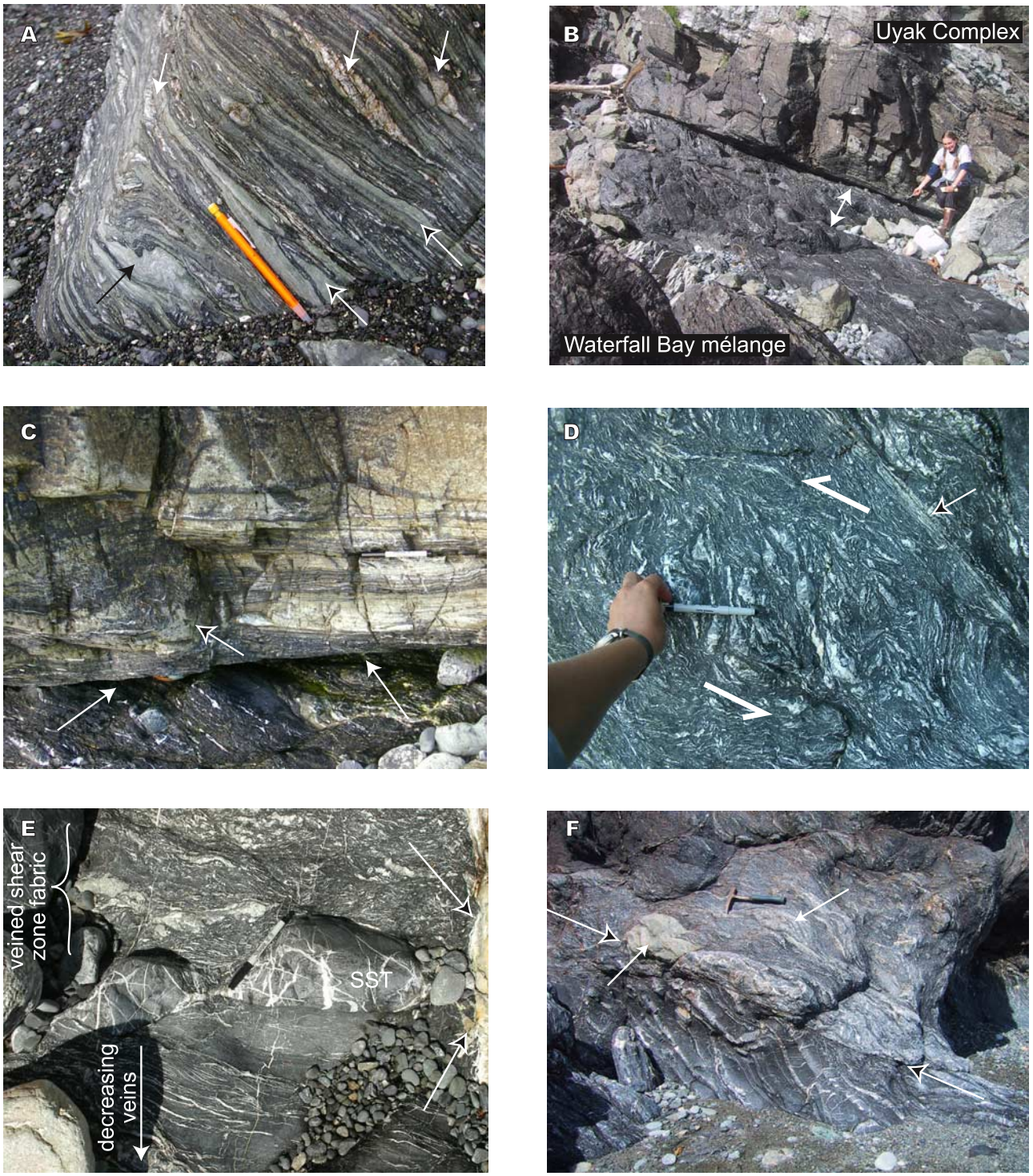

Figure 3

vein precipitation associated with deformational fabrics occurred at 200–250°C and 250–300 MPa [*Myers and Vrolijk*, 1986; *Paterson and Sample*, 1988; *Sample and Moore*, 1987] (Table 3a), consistent with near-peak metamorphic vein precipitation at high-zeolite facies to low prehnite-pumpellyite facies conditions [*Paterson and Sample*, 1988]. The Kodiak Formation is characterized by its pervasive planar cleavage, locally modified by steeply plunging folds, and regionally forming a broad anticlinorium consistent with trench-normal compression across the formation [*Fisher*, 1990; *Fisher and Byrne*, 1987; *Sample and Moore*, 1987]. No metamorphic trends were detected across the formation in a vitrinite-illite study [*Sample and Moore*, 1987], indicating that throw on the intraformational faults was inconsequential after peak metamorphism. Slaty cleavage is mutually crosscutting with duplex faults in the Kodiak Formation, suggesting cleavage formation was coeval with the period of basal accretion [*Sample and Moore*, 1987].

2.5. Waterfall Bay Mélange

[15] The upper several kilometers of the Kodiak Formation suffered discontinuous shearing and flattening deformation, forming the Waterfall Bay mélange (Figure 1) [*Connelly*, 1978; *Fisher and Byrne*, 1987]. *Fisher and Byrne* [1987] reported the thickness of the Waterfall Bay mélange as variable from tens of meters at Uyak Bay to 1 km at Big Waterfall Bay. This study amends the measured thickness at Big Waterfall Bay to at least 3 km, with a gradational basal limit. *Fisher and Byrne* [1987] interpreted this diffuse deformed zone as footwall deformation along the plate boundary décollement during the subduction of the Kodiak Formation during the latest Cretaceous. Deformation in the Waterfall Bay mélange is distinguished by multiple phases of bedding-parallel extension and subvertical compaction (see "stratal disruption" of *Sample and Moore* [1987]). Structures which characterize the mélange are extensional failure of sandstone beds by jointing, normal faulting and cataclastic boudinage with calcite veining in joints and boudin necks, and anastomosing shear/pressure solution fabrics in argillite beds.

3. Uganik Thrust and Its Damage Zones

[16] A sharp and planar surface decorated by deep slickenlines separates the hanging wall and the fault core of the Uganik Thrust (Figures 3b, 3c, and 4i). The 55–65 cm thick fault core is mostly derived from argillites of the Kodiak Formation footwall, cut by a network of Riedel shears and strong, penetrative brittle S-C fabric (Figure 4h). S surfaces are defined by aligned metamorphic chlorite, white mica and rare pumpellyite, and curviplanar pressure solution surfaces. Quartz and calcite veins occur along S surfaces and represent both the rotation of boudins of preexisting veins as well as synshear precipitation. The vein concentration is high in the fault core, but not as high as in the footwall subsidiary faults lower in the damage zone (Figure 5).

[17] The technique of determining slip vectors from S/C fabric intersections was first applied in the damage zones of the Uganik Thrust at Uyak Bay, approximately 130 km along strike from the location of this study [*Moore*, 1978]. The S surface pressure solution cleavage used by *Moore* [1978] was not observed at Waterfall Bay, possibly because of a change in lithology along strike in the Uyak Complex mélange. As in the original study, the orientation of motion on the Uganik Thrust can be measured by strain indicators in the damage zones of both the hanging wall and the footwall, and by slickenlines on the fault surface. The S/C intersection data from the footwall is presented in Figure 4h, with the mean calculated slip vector.

3.1. Hanging Wall Damage Zone: Uyak Complex

[18] Along the Uganik Thrust at the base of the Uyak Complex is a 20–30 cm thick layer of very fine scale banding of Uyak lithologies in a macroscopically ductile fabric (Figures 3a and 3c). Chert beds are reduced to dramatically thinned and pinched asymmetric, internally faulted and stylolitized boudins (Figure 3a). Quartz veins

Figure 3. Field photos at the Uganik Thrust. Pencils and markers in each photo are approximately 15 cm long. (a) Ductile banding in the Uyak Complex (hanging wall damage zone). Asymmetric boudins of gray chert (solid white arrows) are wrapped by stretched bands of green basaltic hyaloclastite (black arrows) and black argillite. Seaward vergent folds are common (black arrow). (b) Uganik Thrust surface at Big Waterfall Bay. Uyak Complex hanging wall damage zone is massive, welded, millimeter-scale banded metamélange. Footwall is characterized by brittle S-C fabrics and abundant veining. Double-headed white arrow shows veined fault core. Planar sharp Uganik Thrust surface is indicated by pointing person. (c) Uganik Thrust contact. Thrust-parallel planar banding characterizes the hanging wall damage zone, while the footwall damage zone is characterized by brittle S surfaces inclined to the thrust surface. White arrows indicate thrust surface. Black arrow indicates small seaward vergent fold. (d) Veined shear zone in footwall damage zone of the Uganik Thrust. Boudins are thinned and folded. There are few throughgoing shear surfaces, as if the entire volumes of the zone deformed as one. A rare throughgoing slip surface (black arrow) is planar, laminated, and sharply crosscuts the veined shear zone fabric. This shear zone is approximately 50 m below Uganik Thrust (Figure 2). Sense of motion is indicated by white arrows. (e) Base of a veined shear zone, fabric ends at boudinaged sandstone bed (SST) at base; deformation is localized above the sandstone bed. High vein density tapers out below sandstone bed, in unsheared argillite. (25 m below Uganik Thrust). Black arrows indicate a large brown quartz vein crosscutting shear zone at edge of photograph. (f) Boudins of dike material included in shear fabric of the largest veined fault (~50 m below the thrust). White arrows indicate boudins of dike material. Black arrows indicate planar shear surface marking base of veined shear zone. Rock hammer for scale ~30 cm.

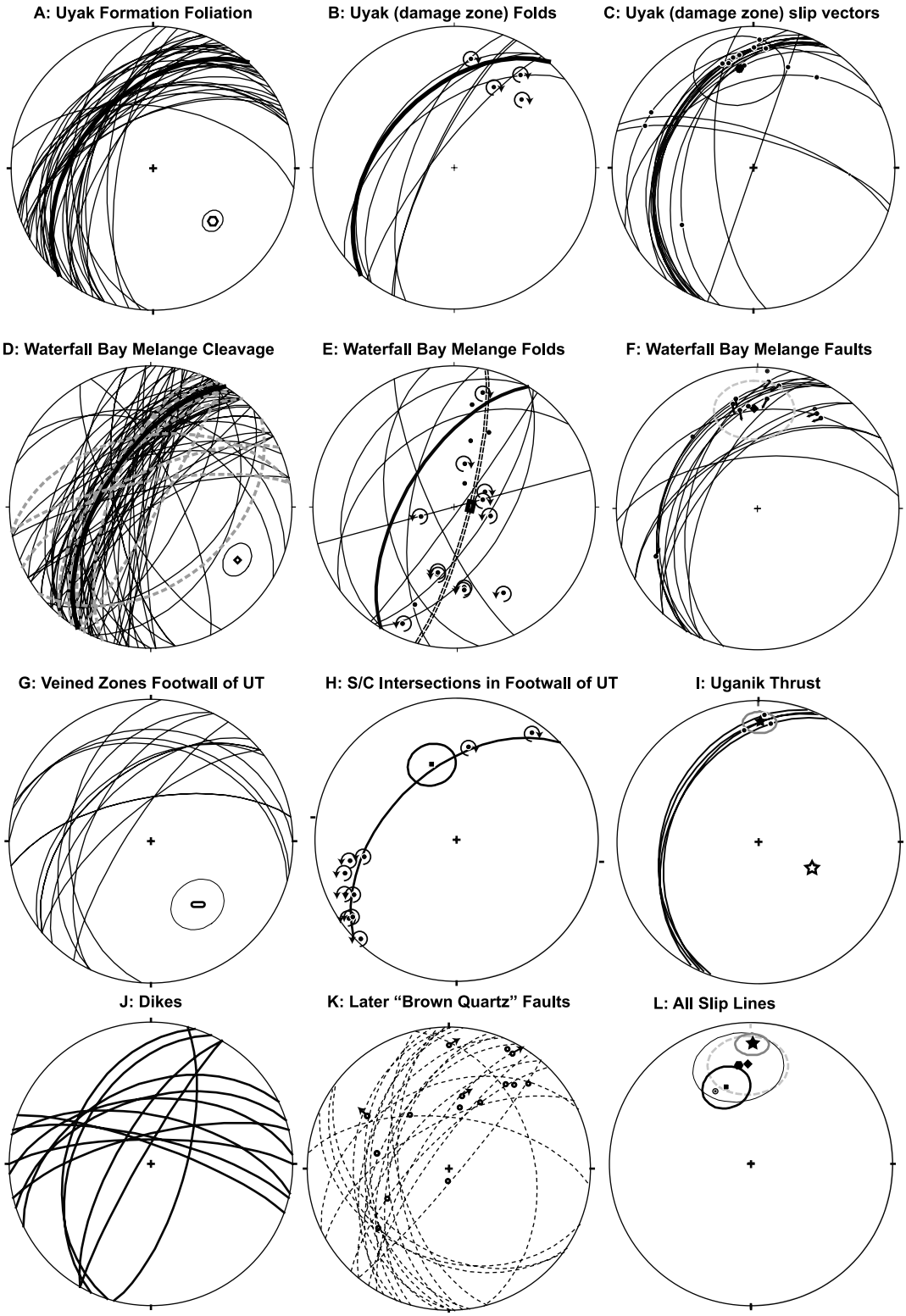
A: Uyak Formation Foliation
B: Uyak (damage zone) Folds
C: Uyak (damage zone) slip vectors
D: Waterfall Bay Melange Cleavage
E: Waterfall Bay Melange Folds
F: Waterfall Bay Melange Faults
G: Veined Zones Footwall of UT
H: S/C Intersections in Footwall of UT
I: Uganik Thrust
J: Dikes
K: Later "Brown Quartz" Faults
L: All Slip Lines

Figure 4

occur along the foliation and cut the foliation at a low angle. Although locally in cherts, textures are suggestive of ductile deformation of quartz, cataclastic flow was the dominant mechanism acting to produce the very fine banding. Granular-ductile folds and boudins are mutually crosscut by pumpellyite- and calcite-filled Riedel shears and joints on the outer surfaces of small folds. Both brittle and ductile deformation mechanisms were active in the hanging wall damage zone during activity on the Uganik Thrust.

[19] Small, seaward vergent folds were measured in the finely banded damage zone (Figures 3a–3c). Folds are highly flattened, having at least one limb and commonly the axial plane subparallel to local banding (Figures 3a and 4b). Fold axes all plunge NE (Figure 4b). Slickenlines were measured on foliation slip surfaces in the banded damage zone (Figure 4c). Lineations cluster in the region of left-oblique thrusting, similar to the motion suggested by fold axes measured by *Moore* [1978].

3.2. Footwall Damage Zone: Waterfall Bay Mélange

[20] The topmost 250 m of the Waterfall Bay mélange are crosscut by densely veined shear zones that generally increase in thickness and frequency up section toward the Uganik Thrust (Figures 3d and 5). These zones have a chaotic fabric and are completely cemented with quartz, yielding an extremely hard fault rock (Figure 3d). The fabric is highly variable, folded and anastomosing, with sandstone boudin size reduced by one to two orders of magnitude compared to the surrounding mélange. The fabric contains boudins of quartz and calcite veins, absent in the surrounding mélange. Boudins are enveloped by a fine-grained, massive argillitic matrix. The weak foliation in the matrix is defined by wavy shear and pressure solution surfaces. Pyrite nodules are common, whereas only individual cubic crystals were observed elsewhere in the footwall. The shear zone boundaries are sharp, but variable in style. Some are bounded by boudins of the Waterfall Bay mélange, as in Figure 3e, where the veined shear zone fabric ends abruptly against the edge of the boudinaged sandstone bed, while the veining intensity gradually declines down section away from the veined zone.

3.3. Deformation and Veining Across the Uganik Thrust

[21] The internal fabric of the footwall subsidiary faults is a veined shear zone lacking systematic shear indicators. The wavy-planar boundaries of the zones are scattered but on average roughly parallel to the Uganik Thrust surface (Figure 4).

[22] Four classes of veins were documented in the Uganik Thrust and its damage zones. The classes were differentiated in the field by mineralogy, color, style and morphology, and crosscutting relations. Field classes were confirmed by fluid inclusion analyses. In order to document vein density distribution, we measured a detailed transect of

Figure 4. Structural data describing Waterfall Bay mélange, Uyak Complex, and the Uganik Thrust. (a) Uyak Formation cleavage surfaces. Thin black lines represent slaty cleavage (n = 35). Bold surface is mean cleavage (221/46.7NW). Pole to mean slaty cleavage surface is shown (open hexagon) with 95% confidence limit of 5.9° (ellipse). (b) Uyak Formation hanging wall damage zone folds. Folds are highly flattened parallel to local banding (thin black lines: axial planes, n = 7). Black dots are fold axes with arrows indicating vergence (n = 4). Fold axes all plunge NE, consistent with rotation toward direction of shear in high strain environment. Bold surface is mean cleavage (same as shown in Figure 4a). (c) Slip vectors in Uyak Formation damage zone. Thin black lines represent shear planes or shear bands within semibrittle banded damage zone. Black dots indicate slip lineations (slickenlines and/or slickenfibers) on those surfaces. Lineations cluster in region of left-oblique thrusting, similar to the motion suggested by fold axes. Mean slip lineation is shown (30/351, black hexagon) with 95% confidence limit of 23° (ellipse). (d) Waterfall Bay mélange cleavage surfaces. Thin black lines represent slaty cleavage (n = 69). Gray dotted lines represent anastomosing shear cleavage (n = 9) which overlap closely with slaty cleavage. Bold surface is mean cleavage (211/61.5NW). Pole to mean slaty cleavage surface is shown (black diamond) with 95% confidence limit (ellipse). (e) Waterfall Bay mélange folds. Bold surface is mean cleavage (same as shown in Figure 4d). Thin black lines are axial planes. Black dots are fold axes with arrows indicating vergence (n = 17). Double bold dash is cylindrical best fit to fold axes (014/79SE). Folds are steepened, and some are overturned. Separation arc is shown with thick-lined black box on best fit (double-dashed) line. (f) Waterfall Bay mélange faults. Black dots are slickenlines with motion shown with black arrows where indicated. Gray bull's-eye is motion on Uganik Thrust as determined percent confidence cone. (g) Boundaries of veined shear zones in footwall damage zone. Mean pole is shown by open bar with 95% confidence ellipse (23°). (h) S/C fabric intersections in footwall damage zone of Uganik Thrust, shown with vergence indicators. Square is mean slip line determined by 90° rotation of intersection point in plane of C surface following *Moore and Byrne* [1987] with 95% confidence cone (13°). (i) Uganik Thrust surface and slickenlines. Mean slickenline (14/000) indicated with black star; 95% confidence limit shown in gray ellipse (7.9°). Pole (55/115) to mean thrust surface (205/35NW) measurement indicated with open star. Ninety-five percent confidence level shown in gray ellipse (2.9°). (j) Small dikes in the field area. No strong preferential orientation is suggested. Dikes did not intrude along regional structural fabric. Post-Uganik Thrust faults (those with layered "brown quartz" veining). (k) Open dots show slickenline and slickenfiber orientations; motion where noted is shown with a black arrow. Most motion indicators suggest dextral normal oblique slip. (l) Summary of slip lines. Black star indicates slicks on the surface of the Uganik Thrust (I). Black square indicates slip line calculated from S/C fabric intersections (Figure 4h). Black diamond indicates slickenlines on faults in the Waterfall Bay mélange (Figure 4f). Black hexagon indicates slickenlines on faults in the Uyak damage zone (Figure 4c). Grey bull's-eye indicates slip vector estimate from *Moore* [1978].

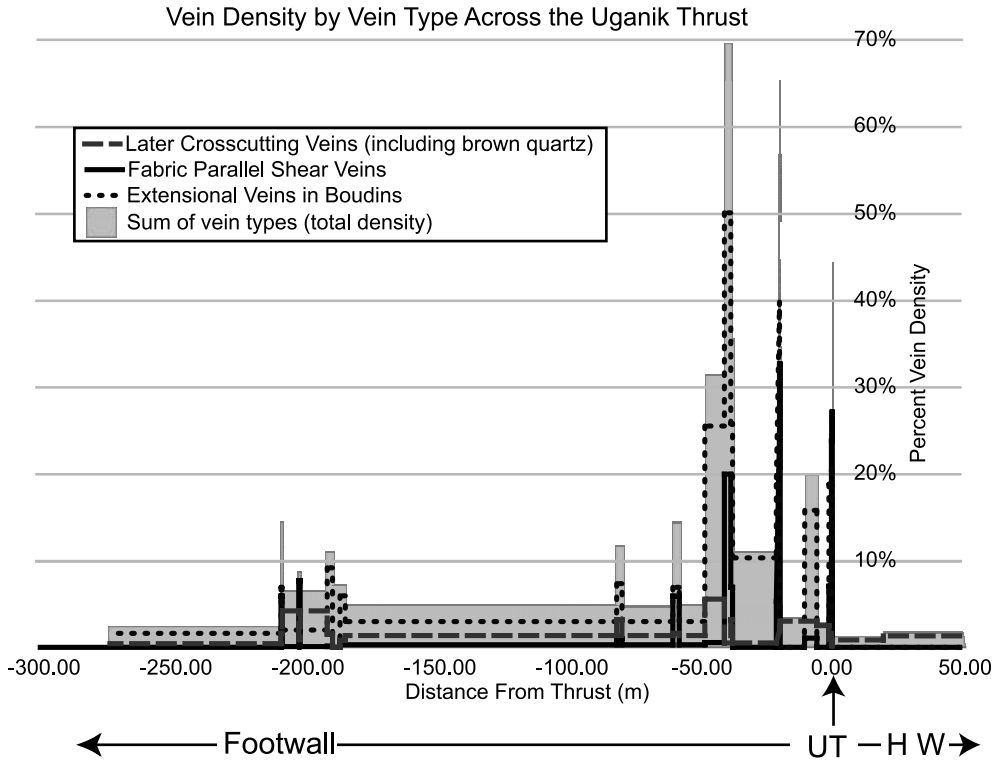

Figure 5. Vein counts across the Uganik Thrust. Solid black line indicates concentration of in-fabric shear veins. Dark gray dashes indicate concentration of later veins (including brown quartz). Black dotted line counts boudin-normal extension veins. Stippled area in background tracks cumulative proportion of rock which is vein material. Two footwall "veined zones" are significantly more veined than the thrust surface itself. (UT, Uganik Thrust surface; HW, hanging wall (Uyak Complex)).

vein counts in 27 discrete zones through the lower 50 m of the Uyak Complex, across the Uganik Thrust, and 284 m down section into the Waterfall Bay mélange (Figure 5). The zone boundaries were determined by visual inspection of the outcrop for changes in deformation scale, style, or apparent vein density (e.g., veined shear zone boundary, Figure 3e). Counts in each zone were performed along a 1 m tape, laid across the outcrop and performed 6 times, rotating the tape approximately 30° each time, to minimize the affect of counting across or along oriented vein sets. Each millimeter mark on the tape was classified as to whether it fell on one of three vein classes or on unveined rock. The measurements at different orientations were averaged to get the mean surface area density of each vein class in each zone. Vein densities are expressed in percentage of millimeter marks on the tape which fell on that vein class. Zones which were thinner than 1 m in outcrop exposure were counted through their thickness and all counts in the zone were made over the same distance. These are presented as a percentage of the length measured. These data should not be extrapolated to volume percentage, and are used here to elucidate relative vein density along the transect.

[23] The first class of measured veins (class 1) are extensional veins at a high angle to bedding or disrupted strata, and were formed during early stages of flattening during burial or subduction of the Kodiak Formation. They are composed of blocky or fibrous quartz, sometimes containing solid calcite inclusions in fibrous quartz crystals. These earliest extensional veins constitute less than 5% of the rock surface area throughout the upper Kodiak Formation (dotted line; Figure 5). Within the subsidiary faults in the footwall damage zone, the concentration of extensional veins increases dramatically to <50% of the rock surface area. These veins are normal to the long axis of sandstone boudins but the boundins in these zones are rotated into an S surface orientation within the fault zones. Because of the geometry of these veins being consistent with the interpreted orientation of extension within the subsidiary faults, and the increased concentration within shear zones, these veins are considered to have formed during Uganik Thrust motion. The origin of most individual veins cannot be tied with certainty to one stage of deformation, therefore, these veins were counted together as one class.

[24] The second and third classes (classes 2 and 3) are fault-parallel veins, most of which are shear veins (e.g., Figure 3d). These are kinematically consistent with the subsidiary footwall faults and lie in S planes and C planes within the fault fabric. They are essentially absent outside these footwall faults. These veins contain quartz and rare pyrite crystals. Since the hanging wall and footwall may have experienced a similar stage of deformation at different times, the shear veins of each formation are separated and compared during fluid inclusion studies (below). Since they are spatially discrete, they appear as a one count in Figure 5.

[25] The final class (class 4) comprises all later veins that crosscut mélange fabrics, Uganik Thrust fabrics, and later intrusives (Figure 3e). The veins have layered crack seal textures and are composed of white quartz, brown quartz, and calcite, with variable slickenfibers on individual layers. Cements of similar mineralogy occur in local breccias associated with dikes. The slightly elevated occurrence of later veins in the footwall subsidiary faults is attributed to the increased brittle strength in those zones due to prior extensive quartz veining. Their orientation is unrelated to all subduction-related fabrics (Figure 4k).

3.4. Constraints on Thrust Motion

[26] A string of dikes, sills, and plutons intruded the accretionary wedge during the early Paleocene owing to subduction of a spreading ridge [*Bradley et al.*, 2000; *Moore et al.*, 1983]. A dike from Malina Bay on Afognak Island near the site of this study gives a hornblende Ar^{40}/Ar^{39} age of 52.3 ± 2.2 Ma [*Bradley et al.*, 2000] so this will be taken as the age of intrusives in the area. As described by *Farris et al.* [2006], the geometry of the intrusives suggests little sensitivity to preexisting structure, and the dikes at Big Waterfall Bay crosscut the fault and earlier cleavages with no apparent relationship to local fabrics (Figure 4j). Thirteen dikes were recorded in the ~250 m cross section (Figure 2c). The main dike found in the study area is 9.5 m thick (Figure 2) and the remaining 12 dikes are less than 1 m thick, usually on order 20 cm, too small to appear on the map or cross section in Figure 2.

[27] Locally, last motion on the Uganik Thrust and its subsidiary footwall faults occurred concurrently with the intrusion of the Afognak dikes. This is demonstrated by the inclusion of clasts of dike material into two of the subsidiary faults in the Uganik Thrust footwall (Figure 3f) and the dike crosscutting the Uganik Thrust itself with only about 10 cm offset (Figure 2c). No thermal aureole was observed around dikes at Big Waterfall Bay, where the intrusions are smaller than those with greenschist facies metamorphic halos described elsewhere in the complex [*Farris et al.*, 2006; *Paterson and Sample*, 1988].

[28] While giving excellent age control on the fault motion, these field relationships raise the question of local perturbation of thermal indicators collected in the vicinity of the dikes. Near the Kodiak Batholith, maximum metamorphic aureole temperatures were 650°C and contact metamorphism was associated with ductile deformation of the country rock, even outside the detectable thermal aureole [*Farris et al.*, 2006]. No structural or metamorphic effects could be found in the vicinity of the much thinner dikes at the Uganik Thrust. The lack of evidence for deformation and thermal aureoles around the dikes was confirmed in both illite crystallinity data and vitrinite reflectance data (presented below), as no anomaly in mean values was discovered in proximity to the dikes.

4. Structural and Thermal Evolution

[29] Low-grade metamorphism is particularly complicated to document in metasedimentary rocks [*Underwood et al.*, 1993b]. This is due to sluggish prograde metamorphism and the stability of characteristic low-grade minerals over a wide range of pressures and temperatures. Recent studies have been critical of the exclusive use of illite crystallinity as a geothermometer [*Robinson et al.*, 1990; *Underwood et al.*, 1993b]. Our understanding of the thermal, geochemical, and strain effects on illite "crystallinity" is at best, incomplete [*Giorgetti et al.*, 2000; *Rahn and Mullis*, 2003; *Robinson et al.*, 1990]. This study attempted the approach of *Underwood et al.* [1993b] in comparing illite crystallinity values (IC) to vitrinite reflectance values (%Ro) as a more reliable geothermometer.

[30] Prior work in the Kodiak Formation analyzed the variation in illite crystallinity and vitrinite reflectance values across a ~70 km transect structurally below the Uganik Thrust [*Sample and Moore*, 1987]. This work showed that neither parameter varied systematically across the transect, except that illite 10Å peak broadened, and vitrinite reflectance dropped within a few kilometers of the Uganik Thrust, where cleavage intensity was reduced. Both of these factors would suggest a decrease in either maximum temperature or in burial duration for the structurally uppermost Kodiak Formation. *Sample and Moore* [1987] suggest lower-grade slivers of rock near the fault zone, but as all structural indicators show dominantly thrust motion, it is inconsistent with tectonic models for the Uganik Thrust to invoke a horse terrane of lower grade than either the footwall or hanging wall.

4.1. Degree of Deformation Ranking

[31] A qualitative scale of deformational rank was developed in order to classify the samples in the field. Scale values range from 0 (least deformed) to 6 (most deformed) and the rubric is shown in Table 1. This rubric was developed specifically for the locations studied, to reflect the particular sequences of deformational events identified by field mapping of the Uganik Thrust at Big Waterfall Bay and the footwall damage zone in the Kodiak Formation. The incremental values used in this scale in no way imply a linear increase of deformation between the defined categories, but are simply useful for identifying and measuring localized zones of increased strain and/or fluid flow indicators.

4.2. Illite Crystallinity

[32] Illite crystallinity has been used as a proxy for paleotemperature in argillitic rocks [*Underwood et al.*, 1993b; *Vrolijk and van der Pluijm*, 1999]. However, there are significant limitations to the method due to the wide range of variables that may affect the peak width of the illite 10Å peak, including time-temperature path, protolith chemistry, and shear or pressure solution fabric development [*Underwood et al.*, 1993b; *Vrolijk and van der Pluijm*, 1999].

[33] Samples were prepared for XRD analysis using the methodology of S. J. Wyld and J. W. Rogers (Preparing phyllite/slate sample for XRD analyses (illite crystallinity) and whole rock $^{40}Ar/^{39}Ar$ radiometric dating, unpublished instructions, 1998). X-ray diffraction spectra for illite crystallinity measurements were collected with CuKα radiation

Table 1. Deformation Ranking

Rank	Description
0	No detectable deformation in hand sample. Coherent, planar bedding with no evidence of pressure solution.
1	Pressure solution cleavage present. In sandstones this may manifest as semiplanar dissolution seams and may result in flaggy cleavage. Best observed as slatey cleavage in argillite. This is typical of the Kodiak Formation regionally.
2	Pressure solution cleavage and stratal disruption. Evidenced by boudinage and normal faulting of sandstone beds. Argillite cleavage is typically wrapped around edges of sandstone beds, but otherwise, cleavage is typically planar. Calcite and/or quartz veins may be present in tension fractures in sandstone and around boudin necks.
3	Shear fabrics, pressure solution cleavage, and disrupted strata present. Shear fabrics typically manifest as S/C fabric development in argillites including cleavage on a smaller spatial scale than the pressure solution cleavage. Slickenlines appear on argillite surfaces. Sandstone fragments are locally rotated, which is clearly displayed from the rotation of earlier bedding-normal tension veins.
4	Characteristic of 3 present, in addition, extensive development of calcite, quartz, or chlorite veins along shear surfaces. Veins may crosscut pressure solution cleavages at a low angle and many are also deformed by pressure solution. Veins occur most commonly as lenses in S surfaces and are commonly slickenlined.
5	Similar to structures described in 4 but the fabric is more deformed. Remnant sandstone boudins are dramatically smaller and often folded and brecciated locally. Quartz veins bound remnant sandstone bodies. Argillite is no longer fissile along cleavages and the whole assemblage is cemented solidly with quartz. Characteristic of footwall subsidiary faults below the Uganik Thrust.
6	Areas classified as ''fault core.'' In the brittle realm this includes cohesive cataclasites and quartz-cemented cataclasites. These tend to be uniform in cataclasic grain size and are derived of a mix of material from the hanging and footwalls of the fault.

at 20 V and 40 mA with a 0.5 diffraction slit, 0.01° steps and count times of 1 second per step. Each sample slide was run three times to determine repeatability. XRD spectra were analyzed using ''MacDiff'' 4.2.2 (Petschick, copyright 1991–2000). The Kübler Index (the width of the peak at half of maximum height (FWHM)) was measured following *Kübler and Jaboyedoff* [2000] and *Wang and Zhou* [2000].

[34] Seven samples of hanging wall damage zone rocks were analyzed. Two of the seven samples contain no white mica peaks at 10Å. Forty-two samples of the Kodiak Formation footwall were analyzed. The illite crystallinity values (FWHM; inverted scale) of these analyses are shown relative to distance below the thrust in Figure 6a. The FWHM varied from 0.303 to 0.471 $\Delta°2\theta$ across the transect, with the mean at 0.394 $\Delta°2\theta$. Duplicates of prepared samples and XRD runs on the same samples produced no significant change in variability along the transect. The variance between samples decreased away from the fault core, but as sampling density also decreased this may be an artifact.

[35] The illite 001 peak width varies erratically along the transect. In order to test whether bulk rock composition has an effect on illite peak width, the ratio of the illite 001 and chlorite 002 peak areas was compared to illite peak width. The illite peak width does not correlate to the illite-to-chlorite ratio ($R^2 = 0.0016$). A general linear model using JMP (version 5.0.1a) also shows no correlation (GLM; $R^2 = 0.04$, $F = 1.7$, $p = 0.20$).

[36] Values of illite crystallinity generally change in response to deformation state. The highest IC values all coincide with veined fault cores. Only one veined fault core, the farthest structurally down section, does not show a corresponding spike in illite crystallinity. A one-way ANOVA was used to test for differences in illite crystallinity relative to the ''degree of deformation'' categories described above. Although a general trend can be observed in the data 6B, the whole model was not significant. Post hoc pairwise comparisons using Tukey's test revealed significant difference in illite crystallinity values only between class 1 (background) and class 6 (fault cores) (whole ANOVA model: $F = 1.89$, $p = 0.11$; class 1 versus 6 distinguishable by Tukey's test; $p < 0.05$). It must be noted that the population of some categories is quite small, as is the total range of illite crystallinity values, therefore statistical significance is less likely. This methodology would be more definitive in a study that encompassed greater spatial area, greater thermal contrast, or more certainty in heating duration in order to detect fault heating/shearing effects.

4.3. Vitrinite Reflectance

[37] The thermal maturity of an organic-bearing sedimentary rock can be effectively estimated by measuring the reflectance of woody tissue. Vitrinite reflectance is strongly related to temperature in the range of about 60°C to about 250–300°C [*Barker and Pawlewicz*, 1986]. Although conventional analyses in passive basins have demonstrated strong correlation between burial heating and coal rank (measured as %Ro), evidence suggests that other factors, notably shear heating and/or hydrothermal fluid circulation, can also effect coal rank [*Barker*, 1988; *Hower and Gayer*, 2002].

[38] Comparisons between vitrinite reflectance and illite crystallinity tend to display considerable scatter but yield meaningful correlations over broad ranges of thermal maturity [*DiTullio et al.*, 1993; *Ohmori et al.*, 1997; *Underwood et al.*, 1993a]. *Underwood et al.* [1993a] were able to relate a broad suite of illite crystallinity and vitrinite reflectance data across the Shimanto Belt in SW Japan, and thereby calibrate the illite crystallinity thermometer for those particular rocks.

[39] Two Uyak Complex samples and fourteen Kodiak Formation samples were analyzed by J. Hower at the Center for Applied Energy Research, University of Kentucky. The Uyak Complex samples yielded no useable vitrinite material. One footwall sample yielded few, widely scattered values; this result is not reliable. The remaining samples were taken from the main fault surface, subsidiary footwall

faults (core), the background footwall Kodiak Formation, and adjacent to an intrusive dike (Figures 6c and 7 and Table 1). Hower measured random reflectance (%Ro) (polarized) for 3–34 grains on each rock sample. The scarcity of vitrinite in the rock made it difficult to increase the number of measurements per sample, which are in some cases too low to produce a statistically significant value. The mean value for each sample is taken as %Ro which varies from 3.7–5.0% across the transect. The standard deviation of measurements within a sample is quite high (0.6% mean standard deviation) but between mean values for samples in the same set is relatively low (0.1–0.3%) (Table 2).

[40] Vitrinite data are displayed relative to the illite 001 FWHM in Figure 6c. As the footwall samples are all similar lithologies from a small area, they all have similar illite crystallinity values (0.41 ± 0.02 $\Delta^\circ 2\theta$). The mean vitrinite %Ro values from this sample population also show little variation (4.47 ± 0.34 $\Delta^\circ 2\theta$), therefore they do not define a line relating IC to %Ro. The two fault core populations are slightly higher in thermal maturity than the cluster defined by the background samples. The sample shown with an open dot (Figure 6c) was collected from an intrusive dike contact in the Waterfall Bay mélange. The value for this sample lies within the general population; there is no evidence for perturbation of vitrinite or illite due to heating proximal to this dike. The ratio of vitrinite values to IC of the Kodiak Formation rocks at the Uganik Thrust is higher than the ratio in the Shimanto Complex rocks (Figure 6c) [*Underwood et al.*, 1993b]. One possible explanation for the difference lies in the short equilibration times for vitrinite reflectance versus that for illite crystallinity [*DiTullio et al.*, 1993; *Hower and Gayer*, 2002], as the Kodiak Formation has been shown to have an extremely brief burial duration, perhaps only 2–4 Ma [*Sample and Reid*, 2003]. Given the short burial duration, we consider heating duration when interpreting vitrinite reflectance values for paleotemperature. Given the same reflectance value, an equation which incorporates a shorter heating duration will result in a higher calculated peak temperature. *Sweeney and Burnham* [1990] give suitable time-dependent equations:

$$T(^\circ C) = 174 + 93^* \ln(\%Ro)$$

for a burial time of 1 Ma, and

$$T(^\circ C) = 158 + 90^* \ln(\%Ro)$$

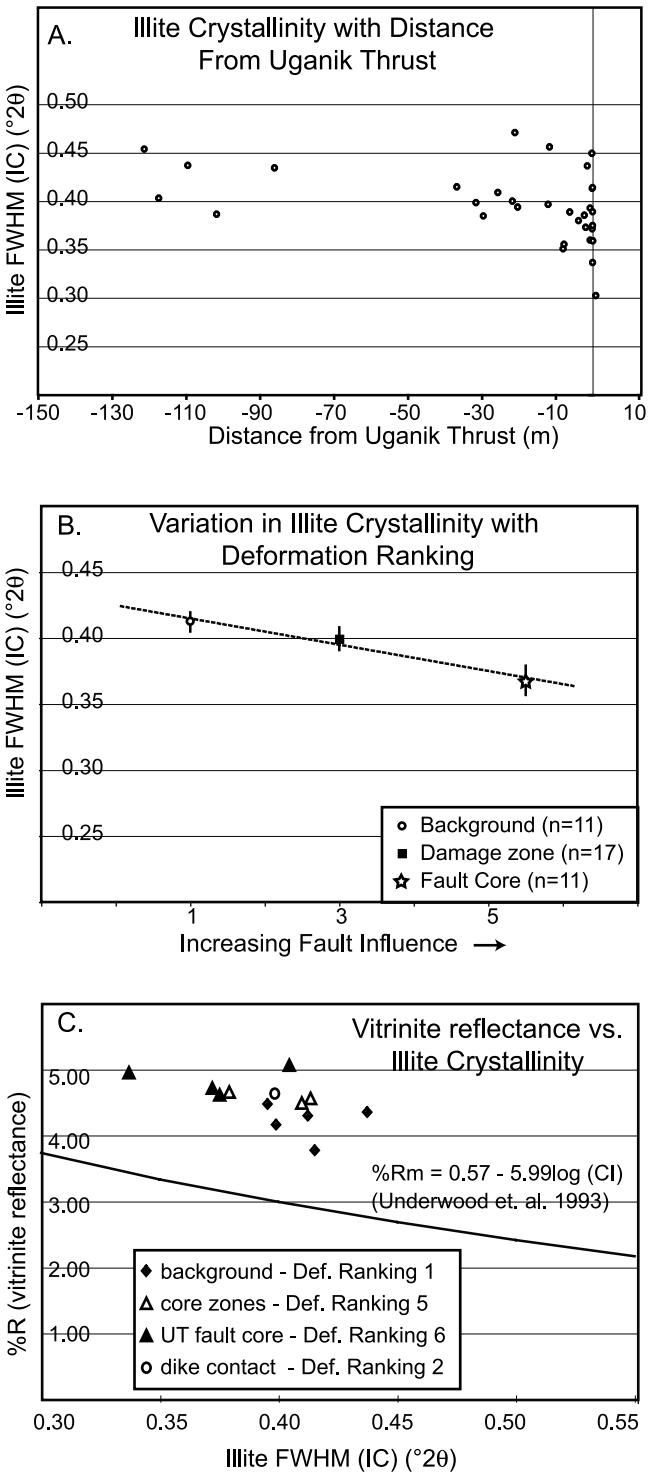

Figure 6. Illite crystallinity data. (a) FWHM (IC) with distance from the Uganik Thrust. Vertical axis is FWHM, peak width increasing (therefore, temperature estimate decreasing) upward on this graph. Maxima and variation increase (and minima decrease) near the Uganik Thrust (0 m on horizontal axis). (b) FWHM (IC) with "deformation rating." Error bars are 1 standard error ($\sigma/\sqrt{n}$). (c) Vitrinite reflectance versus illite crystallinity. Footwall damage zone core samples (open triangles) fall between Uganik Thrust core samples (black triangles) and background (black diamonds). The dike wall sample (open circle) is consistent with background samples. The samples of this study have a higher vitrinite reflectance value for the same illite peak width as reported for the Shimanto Belt. Relationship of *Underwood et al.* [1993a] is shown. See text for discussion.

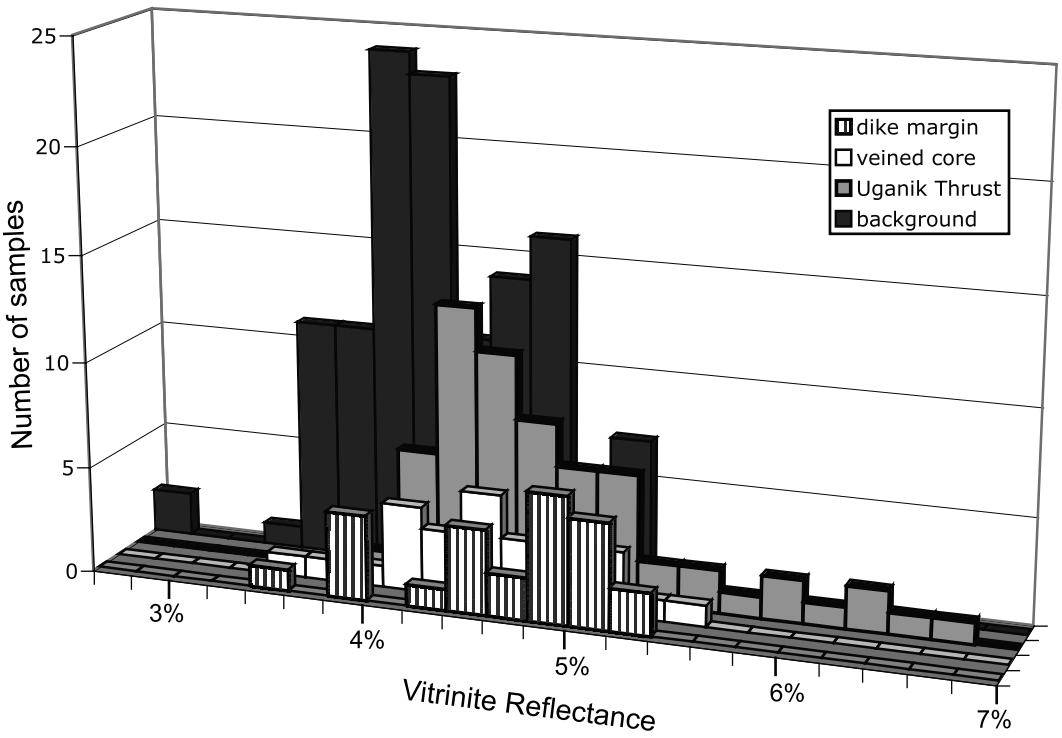

Figure 7. Vitrinite data histogram. All data shown (these are average, not maximum reflectance.) Bins are 0.20% Ro wide. Black bars represent "background" samples (deformation ranking 0–1). Uganik Thrust samples (gray bars) from main fault core (deformation ranking 6). "Veined core" samples (white bars) are deformation ranking 5, these are from other veined zones in footwall damage zone. Striped bars ("dike margin") are a sample of deformation ranking 2 that was collected at the contact of an intrusive dike. Within statistical significance, the "dike" sample is identical to background samples, indicating that heating due to the intrusions was insufficient to reset vitrinite reflectance in the country rock.

for a burial time of 10 Ma. The mean vitrinite reflectance values for each set of samples are used to calculate maximum paleotemperatures (Table 2). The difference in the two heating times produces a difference in maximum paleotemperature estimate of 20°C.

4.4. Raman Spectroscopy of Organic Material

[41] Raman spectroscopy measures the degree of organization of carbonaceous material during its transition to graphite in the range of 330–650°C [*Beyssac et al.*, 2004]. Since the organization of carbon into graphite is not reversible during retrograde metamorphism, this method records peak temperatures [*Beyssac et al.*, 2002]. Absolute temperatures have been measured to within ±50°C and temperature changes of 10–15°C are discernable between samples [*Beyssac et al.*, 2004].

[42] Five polished thin sections of Uyak Complex hanging wall damage zone were analyzed by Olivier Beyssac at the Centre National de la Récherche Scientifique, École Normale Superior, Paris. All samples yielded useable carbon material, and Raman spectra were consistent within and between samples. The degree of graphitization was below the lower limit of the thermometer calibration. Therefore, 330°C is taken as an upper bound on the maximum temperature experienced by the Uyak Complex.

5. Fluid Evolution Before, During, and After Activity on the Uganik Thrust

5.1. Depth and Geothermal Gradient During Cretaceous Subduction

[43] *Vrolijk* [1987b] and *Vrolijk et al.* [1988] reported trapping temperatures from cogenetic water and methane inclusions in synsubduction quartz veins of the Uyak Complex and the landward belt of the Kodiak Formation (Table 2). The samples come from strata-normal quartz veins formed by extension during décollement shear, correlative to our extension veins (class 1). These veins most likely formed at or near the greatest depth of burial of the units. They report fluid conditions of 280 ± 20°C and 330 ± 30 MPa for the Uyak Complex and 240 ± 20° and 300 ± 30 MPa for the Kodiak Formation [*Vrolijk*, 1987b; *Vrolijk et al.*, 1988] (Table 3a). If the overburden density is estimated at 2500 kg/m^3 [*Vrolijk et al.*, 1988], and measured pressure

Table 2. Vitrinite Reflectance Temperature Calculations[a]

	Background	Footwall Faults	Uganik Thrust Core
N	5	3	4
Average measurements per sample	21–30; mean 25	5–12; mean 9	3–35; mean 16
Mean random vitirinite reflectance (%Ro)	4.2	4.5	4.8
Standard deviation (%Ro)	0.3	0.1	0.2
T(°C) for 1 Ma heating time	310	320	320
Uncertainty calculated from the standard deviation of %Ro (°C)	6	1	4
T(°C) for 10 Ma heating time	290	290	300
Uncertainty calculated from the standard deviation of %Ro (°C)	6	1	4

[a]For 1 Ma, $T = 174 + 93 \times \ln(\%Ro)$. For 10 Ma, $T = 158 + 90 \times \ln(\%Ro)$. See *Sweeney and Burnham* [1990].

is assumed to be lithostatic, the maximum depth of subduction of the units can be estimated. Uyak Complex depth is calculated at 13 ± 1.5 km resulting in a calculated geothermal gradient of 20 ± 4°C/km during vein precipitation. The Kodiak Formation estimated depth is 12 ± 1.5 km and the geothermal gradient 20 ± 3.5°C/km. The sedimentary ages of these formations are early mid Cretaceous (Uyak) and latest Cretaceous (Kodiak). Therefore, this relatively low thermal gradient (~20°C/km) is probably representative of shallow to midcrustal conditions on the subduction thrust during long-lived stable Cretaceous subduction.

5.2. Fluid Inclusions in Uganik Thrust-Related Veins

[44] Heating and freezing experiments were performed on four populations of quartz veins (Figure 8). The four populations of quartz veins are: the early, synsubduction extension veins in boudins, Uganik Thrust-related shear veins of the hanging wall damage zone, Uganik Thrust-related shear veins of the footwall damage zone, and postfaulting veins composed of "brown quartz."

[45] Full-sized doubly polished sections were optically mapped before being broken down into small chips for analysis. Heating and freezing analyses were performed at Smith College using the Linkam Examina stage controlled by Linksys software. The system is precise to 0.1°C in both heating and cooling experiments and calibration samples were measured to within 0.2°C of stated values. Optical fluid inclusion petrography detected few gas-phase inclusions and no inclusions formed visible ice at −182°C, the freezing point of methane, nor at −80°C, the freezing point of CO_2. The absence of methane inclusions was confirmed by IR spectroscopy (Q. Williams, personal communication, 2006). Criteria for establishing primary inclusions followed *Roedder* [1984] and *Goldstein* [2003]. No euhedral growth shape assemblages were found in any sample. Most of the measured inclusions are solitary; many have negative crystal shapes indicating they have not been necked down. No inclusions near a crack or planar array of fluid inclusions were measured. Replacement textures suggest that both quartz and calcite veins may dissolve and reprecipitate or replace one another many times during subduction and deformation of a sedimentary package. Only pristine veins lacking replacement textures were measured in this study.

[46] Extensional quartz veins (class 1, Table 3a) consisted of blocky, irregular 100–1000 μm crystals containing significant populations of solid calcite inclusions, suggesting that the quartz might have replaced solid calcite. However, clearer, smaller (50–500 μm), more angular blocky quartz grains which lacked calcite inclusions were found along the vein–wall rock margin and selected for study. These precipitated from an aqueous fluid during or after the replacement of earlier calcite veins, therefore representing a late stage in bedding-parallel extension. A few measured inclusions occurred in three-dimensional

Table 3a. Subduction-Related Veins: Boudin Ends, Tension Joints[a]

	Uyak Complex				Kodiak Formation											
	A1	A2	B1	B2	B3	B4	B5	B6	B7	C1	C2	C3	C4	C5	C6	C7
Aqueous Th (°C)	290	290	280	270	250	215	235	255	250	320	293	288	284	276	267	262
1σ	20	20		20		20	20	20		32	32	32	32	32	32	32
CH_4 pressure (MPa)	330	265	335	345	260	270	330	310	310							
1σ	30	25		38	17	16	25	17								
Salinity (% NaCl eq)										1.9	2.9	1.9	3.1	2.7	1.9	2.9
Depth (km)	13.5	10.8	13.7	14.1	10.6	11.0	13.5	12.7	12.7							
Gradient (°C/km)	21.5	26.8	20.5	19.2	23.6	19.5	17.4	20.2	19.8							

[a]A1 refers to the first sample from source A. Data A are from *Vrolijk et al.* [1988], data B are from *Vrolijk* [1987], and data C are from this study. The mean temperature for the Uyak Complex is 280°C, and mean depth is 13 km. The mean temperature for the Kodiak Formation from *Vrolijk* [1987] is 240°C, and the mean depth is 12 km. The mean temperature for the Kodiak Formation from this study is 280°C, and the mean salinity is 2.5%.

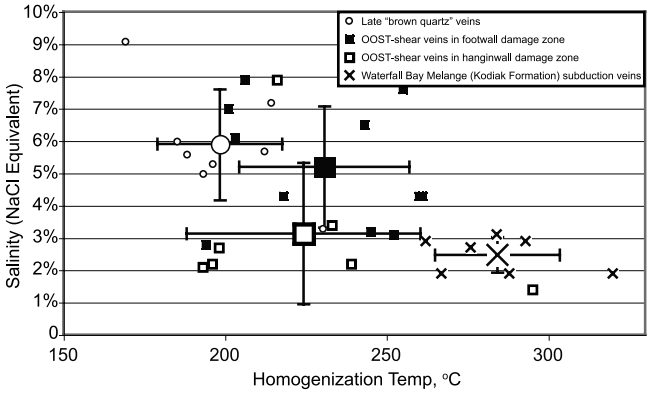

Figure 8. Fluid inclusion populations. Small symbols show individual data points, mean of each data set is shown in large symbol with one standard deviation error bars in each salinity and homogenization temperature. See text for discussion.

clouds in the center of crystals; at least one of these "clouds" had roughly euhedral boundaries. The measured inclusion size of the extensional veins was on order 2–30 μm and bubble proportion at room temperature was consistently estimated at 20–30%. Ninety-four measured inclusions in seven thin sections gave a mean homogenization temperature of 285 ± 20°C (one standard deviation) and salinity of 2.5 ± 0.5% NaCl equivalent (Table 3a).

[47] Fault-parallel veins (classes 2 and 3, Table 3b) are blocky to fibrous quartz with local chlorite. Calcite occasionally occurs as late crystallizing pore fills intergrown with subeuhedral quartz grains but was not found as solid inclusions within any quartz crystal. The density of healed fractures is high within blocky crystals, resulting in difficulty establishing the primary assemblages of fluid inclusions. Measured inclusions were about 1 order of magnitude larger than those found in healed fracture or grain boundary contacts. They had convex surfaces although negative crystal forms were not observed.

[48] In the hanging wall (class 2), a total of 37 measurements were acquired on seven thin sections, giving a mean homogenization temperature of 225 ± 35°C and salinity of 2.3 ± 2% (NaCl equivalent). The salinity was widely variable with measured values ranging from 7.9% (high) to 1.4% (low) (Table 3b).

[49] In the footwall (class 3, Table 3b), a total of 48 measurements were made on eleven thin sections. The mean homogenization temperature is 230 ± 25°C and the salinity is 5.3 ± 1.8%. The salinity is higher than in class 2, although the temperature is similar. Note that 2 and 3 are expressed by one continuous line in 5.

[50] The later veins (class 4, Table 3c) consist of blocky to fibrous, white to orange to brown quartz. They often show evidence of crack-seal growth with variably oriented slickenlines on each crack surface. The aqueous inclusions are large (20–100 μm). Primary inclusion assemblages were usually identified by three-dimensional clouds in the core of crystals. One clear crystal shape outline assemblage was found inside a larger crystal. One hundred eleven fluid inclusions were measured in eight thin sections. Mean homogenization temperature is 200 ± 20°C and salinity is 5.9 ± 1.7% (Table 3c).

[51] Homogenization temperature generally decreases as salinity increases among these populations, and the two factors together define statistically significant differences between the four categories with uncertainty expressed as one standard deviation (Figure 8), suggesting different fluid sources or residence times for fluids present during different stages of deformation.

5.3. Summary

[52] The earliest quartz veins, which are interpreted to have formed during the subduction of the Kodiak Formation and deformation of the Waterfall Bay mélange, have the lowest salinity and homogenize at the highest temperatures (crosses in Figure 8). The fluid inclusion homogenization temperatures from this generation of veins are ~45°C above the trapping temperatures reported by *Vrolijk et al.* [1988] for the same generation of veins. The low salinity of the fluids is consistent with the findings of *Vrolijk et al.* [1988]. Freshening of pore water is common in modern subduction zones [*Kimura et al.*, 1997; *Silver et al.*, 2000; *Torres et al.*, 2004; *Kastner et al.*, 1991]. A probable source of the fluids which precipitated the Kodiak Formation extensional veins during subduction is mineral dewatering in the oceanic crust and subducting sediment, with fluid transport updip within the décollement.

[53] The second and third classes of veins (squares, Figure 8) display no crosscutting structural relationships, as they are spatially separated on either side of the Uganik Thrust. The homogenization temperatures in hanging wall

Table 3b. Syn-Out-of-Sequence Thrusting on Uganik Thrust: Shear Veins[a]

	Uyak Complex							Kodiak Formation										
	C8	C9	C10	C11	C12	C13	C14	C15	C16	C17	C18	C19	C20	C21	C22	C23	C24	C25
Aqueous Th (°C)	295	239	233	198	196	193	216	261	260	245	243	255	201	253	218	194	206	203
1σ	36	36	36	36	36	36	36	26	26	26	26	26	26	26	26	26	26	26
Salinity (% NaCl eq)	1.4	2.2	3.4	2.7	2.2	2.1	7.9	4.3	4.3	3.2	6.5	7.6	7.0	3.1	4.3	3.8	7.9	6.1

[a]Mean temperature is 220°C for the Uyak Complex and 230°C for Kodiak Formation. Mean salinity is 2.5% NaCl eq for Uyak Complex and 5.3% NaCl eq for Kodiak Formation.

Table 3c. Postintrusion, Postfaulting Veins for Brown Quartz Veins and Breccia Cements[a]

	Kodiak Formation							
	C26	C27	C28	C29	C30	C31	C32	C33
Aqueous Th (°C)	230	212	214	193	195	188	185	169
1σ	19	19	19	19	19	19	19	19
Salinity (% NaCl eq)	3.3	5.7	7.2	5.0	5.3	5.6	6.0	9.1

[a]Mean temperature is 200°C. Mean salinity is 5.9% NaCl eq.

and footwall veins of this generation are equivalent (225 ± 35°C and 230 ± 30°C, respectively) but the salinity of the two classes is different (2.3 ± 2% and 5.3 ± 2%, respectively.)

[54] The final generation of veins (class 4; circles, Figure 8) crosscut the dikes that overlap in time with the cessation of Uganik Thrust motion. These have lower mean homogenization temperature (200 ± 20°C, Figure 8, circles) and higher salinity (5.9 ± 2%) than the prethrusting or synthrusting veins, although they are equivalent to thrust-related veins within one standard deviation. The veins contain iron sulfide minerals in addition to quartz and calcite.

[55] These data suggest a trend of decreasing homogenization temperature and increasing salinity through time. The salinity trend can be explained if the locus of fluid flow moved down section relative to the fault through time, coinciding with the introduction of a new fluid source to the fault system. Since the brittle-ductile banded rock of the hanging wall damage zone is dense and without open fractures, we suggest that its formation was a strain-hardening process, resulting in subsequent focusing of deformation and fluid flow into the brittle, fractured footwall damage zone. We further suggest a downward propagation of the primary fluid flow channel over the lifetime of the Uganik Thrust. Down stepping of the thrust fault might relate to a transition from freshening waters derived from sedimentary mineral dehydration to tapping higher-salinity pore waters in the igneous layers of oceanic crust. Alternately, the onset of ridge-trench interaction may have introduced new fluid sources to the system.

[56] The homogenization temperatures of the younger fluid inclusions are lower than older ones, consistent with thrust fault activity at shallowing levels of the wedge, and/or with shallowing of the fluid source during continued fault activity. The uplift is correlated with the timing of ridge subduction and associated igneous activity.

6. Discussion

6.1. Structural History of the Uganik Thrust

[57] The sequence of deformational events experienced by subducting sediments follows a similar evolution across many subduction complexes [*Fisher and Byrne*, 1987; *Jeanbourquin*, 2000; *Moore and Wheeler*, 1978; *Orange et al.*, 1993]. As noted by *Vrolijk* [1985], deformation roughly correlates with times of high water-rock ratios. During initial subduction, the primary deformation events experienced by sediments are flattening and dewatering [*Byrne and Fisher*, 1990; *Moore and Allwardt*, 1980; *Moore and Byrne*, 1987].

[58] The earliest deformation documented by this study was the formation of the Uyak Complex mélange during mid-Cretaceous subduction [*Bradley and Kusky*, 1992; *Byrne*, 1985; *Connelly*, 1978; *Moore*, 1978; *Moore and Wheeler*, 1978]. The Waterfall Bay mélange formed during the subduction and accretion of the Kodiak Formation during the latest Cretaceous (Figure 9a) [*Fisher and Byrne*, 1987]. Duplex fault structures and steeply dipping pressure solution cleavage formed during the underplating of the Kodiak Formation (Figure 9b). The Uganik Thrust cuts the previous deformation at a low angle (Figures 2, 4, and 9c), representing later reactivation along the paleodécollement zone. The very thin granular-ductile damage zone in the Uyak Complex hanging wall likely records the earliest localization of shear strain along the Uganik Thrust. The mechanisms recorded by rare ductile processes in quartz are distinct from the footwall deformation. This ductily deformed, strain hardened zone was subsequently thrust over more shallowly deformed Waterfall Bay mélange, escaping later brittle damage.

[59] Following incorporation into the wedge, the Waterfall Bay mélange may have remained slightly weaker than coherent sedimentary packages accreted on either side. This may have been due to stratal disruption, the rheology contrast between the Kodiak Formation and the Uyak Complex, or the low-porosity Uyak Complex acting as a hydraulic seal. Any or all of these factors could have contributed to localizing the motion of the Uganik Thrust along the latent décollement mélange zone.

[60] The veined subsidiary faults in the footwall of the Uganik Thrust constitute a distinctive style of deformation that can be related to fluid transport in the fault zone. The higher vein concentrations (Figure 5) suggest that aqueous fluids were severely out of equilibrium as they passed through these zones. As calculated by *Vrolijk et al.* [1988], 10^3 to 10^4 water volumes are necessary to deposit one volume of vein quartz. Elsewhere in the Kodiak Formation, *Fisher et al.* [1995] were able to show that local fluid circulation during farfield stress cycling could deposit quartz into fibrous tension veins. That model is not considered applicable to the veined zones at the Uganik Thrust owing to the significant shear deformation compared to the surrounding rock. The order-of-magnitude thinning in boudin size suggests significant comminution and shearing, and the folding, breakage, and recycling of quartz vein material also indicates fault slip. In addition, the thermal and geochemical evolution of these fluids prohibits slow, equilibrium mining of wall rock silica as a mechanism for their formation.

[61] The *Vrolijk* [1987b] and *Vrolijk et al.* [1988] fluid inclusion studies suggest a similar geotherm, but slightly deeper depth and higher temperature during vein precipitation, for the Uyak Complex relative to the Kodiak Formation. However, our results from this study indicate higher temperatures in both vitrinite reflectance data and fluid inclusion homogenization temperatures in the uppermost

Kodiak Formation than previously reported. Previous structural interpretations place our study location at the top of the Kodiak Formation on the limb of a broad regional anticlinorium, and probably the earliest subducted material of that formation [*Byrne and Fisher*, 1987; *Sample and Fisher*, 1986; *Sample and Moore*, 1987], which is not a predicted location for the highest paleotemperatures. The increased paleotemperature in the uppermost Kodiak Formation brings it up to the same temperature (within resolution) as the structurally overlying Uyak Complex, in the vicinity of the Uganik Thrust. Here we explore four possible interpretations for locally high temperatures in the vicinity of the Uganik Thrust, which need not be mutually exclusive.

[62] First, the uppermost Kodiak Formation may comprise a cryptic thrust sheet which was subducted to a different temperature-depth path than the rest of the formation, as suggested by *Connelly* [1978] and *Sample and Moore* [1987]. However, the previously determined trend in illite crystallinity values reported by *Sample and Moore* [1987] suggested an increase of peak width near the top of the Kodiak Formation, a result opposite to the findings of this study. Although this large-scale illite crystallinity anomaly could not be compared with the smaller geographic scale of our study, this pattern could be explained by the affects of increased shear in the Waterfall Bay mélange.

[63] Second, the local occurrence of dikes associated with the Afognak Pluton could be responsible for a thermal aureole. This is rejected on the basis of the absence of measurable anomalies in vitrinite reflectance, illite crystallinity, or fluid inclusion homogenization temperatures in proximity to the small dikes in the study area. *Farris et al.* [2006] reported that the metamorphic aureole for the Kodiak Batholith and related intrusions is about 0.1× the intrusion radius for smaller intrusions, with the factor dropping as intrusions become smaller. The largest intrusion in the study transect crosscuts the Uganik Thrust, and is 10 m thick. According to the relation reported by *Farris et al.* [2006], the

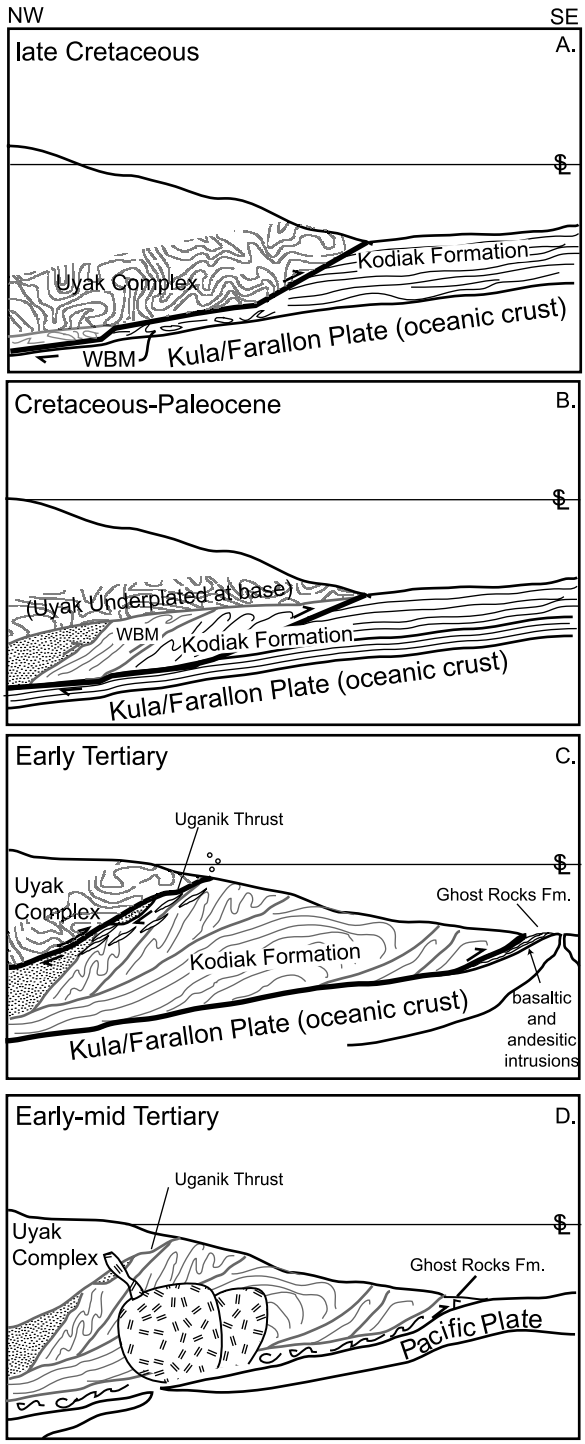

Figure 9. Cartoon of activity on the Uganik Thrust. Active structures are shown in black, while those that are no longer active at each stage are shown in faded gray. (a) Late Cretaceous. Uyak Complex mélange is already incorporated into wedge by basal accretion. Oceanic plate is moving northwest relative to overriding wedge. Kodiak Formation is beginning to subduct, and Waterfall Bay mélange is developing in the décollement zone. Structurally higher parts of the wedge are subaerially exposed, contributing greenstone and blueschist clasts to Kodiak Formation conglomerates. (b) Latest Cretaceous–earliest Paleocene. Subduction and duplex underplating of the Kodiak Formation, with substantial shearing and steep, seaward vergent folding and the development of the formation-wide anticlinorium. (c) Early Tertiary. The paleodécollement has been rotated landward owing to successive underplating of substantial volumes of Kodiak Formation sediment. Out-of-sequence thrusting develops, to thicken the wedge landward of the underplating. At the toe of the wedge, a spreading ridge flank is beginning to subduct. The turbidites deposited on this ridge are intruded by basaltic and andesitic pillow lavas and hyaloclastites, and these materials are underplated (Ghost Rocks Formation). (d) Early mid-Tertiary. Ridge subducts, generating Kodiak Batholith and related intrusions. Magmatic fluids percolate through wedge. Dikes intrude to crosscut Uganik Thrust. Activity on the Uganik Thrust ceases, followed by precipitation of "brown quartz" veins.

metamorphic aureole for this dike would be less than 50 cm. This area was subject to very high sampling density and no trends were detected. Therefore we are confident that local dike intrusions did not create metamorphic aureoles along our study transect which altered the results of illite or vitrinite measurements above background scatter.

[64] Third, heating of the uppermost Kodiak Formation could have resulted from overthrusting of the hotter Uyak Formation along the Uganik Thrust. Because of poor temperature resolution in the Uyak Formation this model cannot be adequately tested. However, the maximum background temperatures given by vitrinite reflectance data in the uppermost Kodiak Formation (290°C for 10 Ma; 300°C for 1 Ma; Table 1) is indistinguishable from previous authors' temperature estimates for the Uyak Complex [*Byrne*, 1985; *Connelly*, 1978; *Kusky et al.*, 1997]. If the Uyak Complex was at or near its maximum paleotemperature when the Uganik Thrust was active, it is possible that it might have contributed to the local temperature anomaly in the uppermost Kodiak Formation. Heating through overthrusting of hotter hanging wall rocks has been observed in similar settings [*Underwood et al.*, 1996].

[65] Fourth, the anomalous heating could have been related to increased geothermal gradient during the subduction of the Kula-Resurrection spreading ridge which occurred locally during the early Tertiary [*Bradley et al.*, 2000; *Farris et al.*, 2003; *Haeussler et al.*, 2003] (Figure 9d) coincident with last motion of the Uganik Thrust. This event was regional and is well recorded throughout the Kodiak Complex by the presence of intrusives and contact metamorphism around plutons. However, no widespread resetting of geothermometers is observed as has been noted in other settings, e.g., thermal resetting of the parts of the Shimanto Complex during Tertiary ridge subduction [*DiTullio and Hada*, 1993; *Sakaguchi*, 1999; *Taira et al.*, 1988] and the thermal overprinting of some Franciscan Complex rocks during the passage of the San Andreas triple junction [*Underwood et al.*, 1996].

[66] The best explanation for the increased paleotemperature of the Waterfall Bay mélange is a confluence of the motion of the Uganik Thrust, and resulting heat/fluid conduit, with the period of increased basal heat flow from the subduction of the Kula-Resurrection spreading ridge. As the geothermal gradient increased in the wedge, the hot Uyak Complex rocks were thrust over the Kodiak Formation and high-temperature fluids migrated up the thrust. The syntectonic thermal peak locally overprinted thermal maturity indicators in the uppermost Kodiak Formation, destroying any detectable thermal gap that would have been caused by throw on the Uganik Thrust. The slight increase in vitrinite reflectance along fault surfaces of the Uganik Thrust damage zone, if significant, could be attributed to a combination of frictional heating, hot fluid flow, or shear-related maturation of the organic material.

6.2. Throw

[67] Thermal and barametric data do not allow absolute determination of the throw on the Uganik Thrust but some constraints can be determined. The Uyak Complex and Kodiak Formation contain synsubduction fluid inclusions which indicate similar homogenization temperatures and salinity, consistent with similar subduction burial histories for the two formations [*Vrolijk*, 1987b; *Vrolijk et al.*, 1988]. The metamorphic mineralogy suggests similar grade (pumpellyite-bearing) [*Sample and Moore*, 1987; *Vrolijk*, 1987a]. The peak hanging wall temperature was less than 330°C. *Vrolijk et al.*'s [1988] results elsewhere in the Kodiak Formation suggest a difference in fluid inclusion trapping temperatures of 40°C. On the basis of the carbon thermometers and fluid inclusion homogenization and trapping temperatures, the thermal gap across the Uganik Thrust is 0–45°C, and between the Uyak Complex and the more typical Kodiak Formation, is on order 50°C. This temperature range (300 ± 20°C) coincides with the low-temperature end of a zone of transition in deformation mechanisms in quartz at geologic strain rates [*Davis and Reynolds*, 1996]. The deformation microstructures present in the Uganik Thrust damage zone in the two units are distinct. The Kodiak Formation (footwall) damage zone was deformed by frictional sliding, pressure solution, and brittle fracture in argillites. The Uyak Complex (hanging wall) damage zone is extremely localized and deformed by cataclasis and granular flow in argillites and greenstone hyaloclastites, and by pressure solution (stylolite formation) and grain boundary migration in cherts and quartz veins. The quartz veins in the Kodiak Formation do not show microstructural evidence of ductile overprinting. The difference in dominant mechanism in the two sides of the damage zone could be attributable to higher temperatures, longer burial duration, or slower strain rate in the Uyak Complex than in the Kodiak Formation. These qualitative observations are consistent with the broader thermal contrast of ~50°C between the Uyak Complex and the Kodiak Formation away from the contact.

[68] The estimated geothermal gradient during the subduction of both the Uyak Complex and the Kodiak Formation is 20°C/km [*Vrolijk et al.*, 1988], suggesting that the depth of subduction of the Kodiak Formation at the time of vein precipitation was ~12 km and the Uyak was ~13.5 km. As the activity of the Uganik Thrust was temporally correlated with magmatic activity and the ridge subduction event, the geothermal gradient was likely much higher, with gradients as high as ~50°C/km recorded by fluid inclusions during ridge subduction in the Shimanto Complex [*Sakaguchi*, 1999]. Using this estimate of ~50°C/km, the throw across the Uganik Thrust and the Waterfall Bay mélange would be less than about 1 km. The paleoorientation of the fault is unknown, but at typical dip angles for OOST we would predict that the total offset is less than 10 km.

6.3. Comparison to Other Fossil OOST

[69] Few prior studies examine similar faults with post-thermal peak offset. Here we present four established ancient OOST of which three show substantial thermal gaps.

[70] Two examples come from the Cretaceous Shimanto Accretionary Complex of SW Japan. The paleoseismogenic Nobeoka Thrust is an OOST with a thermal gap of ~70°C

between the hanging wall and footwall rocks [*Kondo et al.*, 2005; *Okamoto et al.*, 2006; *Tsuji et al.*, 2006]. The Fukase Fault is an OOST with a 50°C thermal gap [*Ohmori et al.*, 1997]. The Irish Canyon Thrust in California's Franciscan Complex is an OOST with a thermal gap of ~45°C [*Underwood and Laughland*, 2001]. The Isthmus Bay thrust is a very small offset, intraformational thrust fault within the Kodiak accretionary complex which shows characteristics of a fluid conduit similar to larger OOST [*Rowe et al.*, 2002; *Thompson*, 2002].

[71] The Nobeoka, Fukase, Isthmus Bay, and Uganik thrust faults occur as discrete fracture surfaces which demonstrably cross cut earlier structural fabrics in the wall rocks at a low angle. The earlier structural fabrics are anastomosing and indicate deformation processes including granular flow, pressure solution, and cyclic reactivation of multiple micro and macrofault surfaces. In contrast to the older fabrics, these faults are discrete brittle zones formed by fresh fracturing of coherent wall rock with little influence from the older rock fabrics. *Ohmori et al.* [1997] showed that the ancient Fukase Fault and the modern OOST in the Nankai Trough both cut rocks 20–30 Ma older than the fault activity. *Kimura et al.* [1997] showed that OOST systematically thicken the area of the accretionary wedge known as the "transition zone," where the age of the rocks will depend on the rate of accretion but will be older by a significant margin than the age of faulting on the OOST. The Isthmus Bay thrust contains aqueous fluid inclusions in breccia-cementing quartz veins which homogenize at 145°C [*Rowe et al.*, 2002] well below the 225°C thermal maximum experienced by the wall rocks [*Vrolijk et al.*, 1988].

[72] The Irish Canyon thrust fault is a more diffuse structure, consisting of a fault-bounded zone of stratal disruption which is offset from the location of the measured thermal gap of 45°C [*Underwood and Laughland*, 2001]. Although the fault zone was not mapped in comparable detail to the others described here, it shares the spatial separation between thermal gap and structural contact that is inferred for the Uganik Thrust. Thrusting of a warm hanging wall over a cooler footwall could be responsible for an asymmetric thermal aureole in the footwall in both cases.

[73] The Uganik, Nobeoka, and Isthmus Bay faults display extreme structural asymmetry, with the footwall damage zone approximately 2 orders of magnitude thicker than the hanging wall damage zones [*Kondo et al.*, 2005; *Rowe et al.*, 2002; *Thompson*, 2002]. Evidence of substantial hydrofracture and veining is pervasive in the footwall damage zone and nearly absent in the hanging wall damage zone. This is consistent across scale when the damage zone is on order 10^4 m (Nobeoka Thrust), 10^{2-3} m (Uganik Thrust) and 10 m thick (Isthmus Bay Thrust). Repeatedly fractured and veined footwall damage zones exist at all three faults, suggesting fluid pressure reached lithostatic pressure repeatedly in the rock volume below the fault surfaces. This highly fractured zone could have been a reservoir for advecting fluids where pressure might build between flow events. When the footwall fractured reservoir zones were fluid-filled, the thickness of zones at both the Nobeoka and Uganik thrusts is on the order of magnitude which could potentially be imaged as negative polarity seismic reflectors.

[74] In the case of the Nobeoka and Uganik thrusts, the fault core itself is fine-grained, low-porosity cataclasite and unlikely to act as a conduit for updip fluid flow. A similar stratigraphy of deformational fabrics was identified in the footwall damage zone of the Nobeoka and Uganik thrusts. The complex crosscutting relationships of veins in the Nobeoka footwall does not suggest any clear migration of the damage zone, but fluid inclusion homogenization temperatures generally decrease down section away from the thrust. This was interpreted by *Kondo et al.* [2005] as evidence for downward migration of primary fluid expulsion channels during OOST activity. The Uganik Thrust shows a similar trend of decreasing homogenization temperatures in aqueous inclusions with time during fault activity. Shear veins are concentrated in discrete footwall faults within the damage zone and no structural crosscutting trends were established. In both cases, the geometries of the complex damage zone vein networks do not reveal very clear spatial organization of vein classes. The diverse orientation of the veins suggests low differential stress during cracking, supporting the hypothesis of high fluid pressure. Therefore, it is possible that the entire vein-rich damage zone had open, fluid-filled fractures at some time, or that the thickness, volume, or density of the open crack network varied over time. Cracks may have become inactive when quartz precipitation filled them, creating the vein network, although crack-seal veins in the Nobeoka thrust damage zone suggest repeated activation. Therefore, the footwall damage zone of each of these thrusts during active movement and fluid transport would most likely consist of a network of quartz veins, cross cut by a network of fluid-filled fractures (transiently open).

[75] The Isthmus Bay thrust, in contrast, has a fault core vein and evidence of rapid precipitation in dilational jogs in both the fault core and footwall damage zone. In this shallower case, the fault surface is a probable candidate for a fluid advection channel during active faulting. This may be an updip analog for active OOST where normal stress is lower than in the other examples.

7. Conclusions

[76] The Uganik Thrust is a fossil out-of-sequence thrust (OOST) or splay thrust which deformed the Kodiak accretionary complex, south central Alaska, during early Tertiary subduction of a spreading ridge. The structural development and thermal anomalies at the Uganik Thrust are comparable to those reported for other fossil OOSTs. Collectively, these provide ancient onland analogs useful in understanding the evolution of active OOSTs.

[77] **Acknowledgments.** The 2004 field campaign to Kodiak and Afognak islands was greatly enhanced by the assistance of Alexander Wells McKiernan, who was supported by Demian Saffer. Fluid inclusion work was performed at Smith College with the generous assistance and supervision of Larry Meinert. X-ray diffraction was carried out by Peter Mueller-Wille. Vitrinite analyses were performed by Jim Hower at the

University of Kentucky, who also provided essential consultation on their interpretation. Quentin Williams used IR spectroscopy to confirm the absence of methane inclusions. Raman spectroscopy on carbonaceous material was measured and interpreted by Olivier Beyssac. John Solum and Mike Underwood provided invaluable assistance with XRD techniques and interpretation. Mike Underwood also provided rigorous reviews and advice that improved this work immeasurably. We thank Gaku Kimura for his thoughtful review. This work was supported by a Geological Society of America Student Research grant to C. Rowe and National Science Foundation grant OCE-0203664 to J. C. Moore. The authors are grateful to Seahawk Air and Kodiak Brewing Company for enabling and enriching the field campaign.

References

Barker, C. E. (1988), Geothermics of Petroleum Systems: Implications of the stabilization of kerogen thermal maturation after a geologically brief heating duration at peak temperature, in *Petroleum Systems of the United States*, edited by L. B. Magoon, *U.S. Geol. Surv. Bull.*, *1870*, 26–29.

Barker, C. E., and M. J. Pawlewicz (1986), The correlation of vitrinite reflectance with maximum temperature in humic organic matter, in *Paleogeothermics: Evaluation of Geothermal Conditions in the Geological Past*, *Lect. Notes Earth Sci.*, vol. 5, edited by G. Buntebarth and J. Lefler, pp. 79–93, Springer, Berlin, Germany.

Beyssac, O., B. Goffe, C. Chopin, and J. N. Rouzaud (2002), Raman spectra of carbonaceous material in metasediments: A new geothermometer, *J. Metamorph. Geol.*, *20*(9), 859–871.

Beyssac, O., L. Bollinger, J.-P. Avouac, and B. Goffe (2004), Thermal metamorphism in the lesser Himalaya of Nepal determined from Raman spectroscopy of carbonaceous material, *Earth Planet. Sci. Lett.*, *225*, 233–241.

Bradley, D. C., and T. M. Kusky (1992), Deformation history of the McHugh Complex, Seldovia Quadrangle, south-central Alaska, in *Geologic Studies in Alaska by the U.S. Geological Survey During 1990*, edited by D. C. Bradley and A. B. Ford, *U.S. Geol. Surv. Bull.*, *1999*, 17–32.

Bradley, D. C., R. Parrish, B. Clendenen, D. R. Lux, P. Layer, M. T. Heizler, and T. Donley (2000), New geochronological evidence for the timing of early Tertiary ridge subduction in Southern Alaska, in *Geologic Studies in Alaska*, edited by K. D. Kelley and L. P. Gough, *U.S. Geol. Surv. Prof. Pap.*, *1615*, 5–21.

Byrne, T. (1982), Structural evolution of coherent terranes in the Ghost Rocks Formation, Kodiak Island, Alaska, *Geol. Soc. Spec. Publ.*, *10*, 229–242.

Byrne, T. (1985), The Uyak Complex: A brittle-ductile shear zone, *Geol. Soc. Am. Abstr. Programs*, *17*(6), 346.

Byrne, T., and D. Fisher (1987), Episodic growth of the Kodiak convergent margin, *Nature*, *325*(6102), 338–341.

Byrne, T., and D. Fisher (1990), Evidence for a weak and overpressured decollement beneath sediment-dominated accretionary prisms, *J. Geophys. Res.*, *95*(B6), 9081–9097.

Carson, B., M. Kastner, D. Bartlett, J. Jaeger, H. Jannasch, and Y. Weinstein (2003), Implications of carbon flux from the Cascadia accretionary prism: Results from long-term, in situ measurements at ODP Site 892B, *Mar. Geol.*, *198*(1–2), 159–180.

Clarke, J., and H. Samuel (1972), Reconnaissance bedrock geologic map of the Chugach Mountains near Anchorage, Alaska, *U.S. Geol. Surv. Misc. Field Studies Map Rep., mf-0350*.

Clarke, J., H. Samuel, and G. A. Carver (1992), Late Holocene tectonics and paleoseismicity, southern Cascadia Subduction Zone, *Science*, *255*(5041), 188–192.

Connelly, W. (1976), Mesozoic geology of the Kodiak Islands and its bearing on the tectonics of southern Alaska, Ph.D. thesis, Univ. of Calif., Santa Cruz.

Connelly, W. (1978), Uyak Complex, Kodiak Islands, Alaska: A Cretaceous subduction complex, *Geol. Soc. Am. Bull.*, *89*, 755–769.

Cummins, P. R., T. Hori, and Y. Kaneda (2001), Splay fault and megathrust earthquake slip in the Nankai Trough, *Earth Planets Space*, *53*, 243–248.

Davis, G. H., and S. J. Reynolds (1996), *Structural Geology of Rocks and Regions*, John Wiley, New York.

DiTullio, L., and T. Byrne (1990), Deformation paths in the shallow levels of an accretionary prism: The Eocene Shimanto belt of southwest Japan, *Geol. Soc. Am. Bull.*, *102*, 1420–1438.

DiTullio, L., and S. Hada (1993), Regional and local variations in the thermal history of the Shimanto Belt, southwest Japan, in *Thermal Evolution of the Tertiary Shimanto Belt, Southwest Japan: An Example of Ridge-Trench Interaction*, edited by M. B. Underwood, *Spec. Pap. Geol. Soc. Am.*, *273*, 103–114.

DiTullio, L., M. M. Laughland, and T. Byrne (1993), Thermal maturity and constraints on deformation from illite crystallinity and vitrinite reflectance in the shallow levels of an accretionary prism: Eocene-Oligocene Shimanto Belt, southwest Japan, in *Thermal Evolution of the Tertiary Shimanto Belt, Southwest Japan: An Example of Ridge-Trench Interaction*, edited by M. B. Underwood, *Spec. Pap. Geol. Soc. Am.*, *273*, 103–114.

Ernst, W. G. (1971), Metamorphic zonations on presumably subducted lithospheric plates from Japan, California, and the Alps, *Contrib. Mineral. Petrol.*, *34*(1), 43–59.

Farris, D. W., P. J. Haeussler, and R. Friedman (2003), Slab-window segmentation and the evolution of the Sanak-Baranof belt: An example from Kodiak Island, Alaska, *Geol. Soc. Am. Abstr. Programs*, *35*(6), 428.

Farris, D. W., P. J. Haeussler, R. Friedman, S. Paterson, R. Saltus, and R. Ayuso (2006), Emplacement of the Kodiak batholith and slab-window migration, *Geol. Soc. Am. Bull.*, *118*(11).

Fisher, D. (1990), Orientation history and rheology in slates, Kodiak and Afognak Islands, Alaska, *J. Struct. Geol.*, *12*(4), 483–498.

Fisher, D., and T. Byrne (1987), Structural evolution of underthrusted sediments, Kodiak Islands, Alaska, *Tectonics*, *6*(6), 775–793.

Fisher, D., S. L. Brantley, M. Everett, and J. Dzvonik (1995), Cyclic fluid flow through a regionally extensive fracture network within the Kodiak accretionary prism, *J. Geophys. Res.*, *100*(B7), 12,881–12,894.

Giorgetti, G., I. Memmi, and D. R. Peacor (2000), Retarded illite crystallinity caused by stress-induced sub-grain boundaries in illite, *Clay Miner.*, *35*(4), 693–708.

Goldstein, R. H. (2003), Petrographic analysis of fluid inclusions, in *Fluid Inclusions: Analysis and Interpretation*, vol. 32, edited by I. Samson, A. Anderson, and D. Marshall, pp. 9–54, Mineral. Assoc. of Can., Quebec, Que.

Haeussler, P. J., D. C. Bradley, R. Wells, and M. L. Miller (2003), Life and death of the Resurrection plate: Evidence for its existence and subduction in the northeastern Pacific in Paleocene-Eocene time, *Geol. Soc. Am. Bull.*, *115*(7), 867–880.

Hower, J. C., and R. A. Gayer (2002), Mechanisms of coal metamorphism: case studies from Paleozoic coalfields, *Int. J. Coal Geol.*, *50*, 215–245.

Ito, Y., and K. Obara (2006a), Dynamic deformation of the accretionary prism excites very low frequency earthquakes, *Geophys. Res. Lett.*, *33*, L02311, doi:10.1029/2005GL025270.

Ito, Y., and K. Obara (2006b), Very low frequency earthquakes within accretionary prisms are very low stress-drop earthquakes, *Geophys. Res. Lett.*, *33*, L09302, doi:10.1029/2006GL025883.

Jeanbourquin, P. (2000), Chronology of deformation of a Franciscan melange near San Francisco, *Ecologae Geol. Helv.*, *93*, 363–378.

Kastner, M., H. Elderfield, and J. B. Martin (1991), Fluids in convergent margins: What do we know about their composition, origin, role in diagenesis and importance for oceanic chemical fluxes, *Philos. Trans. R. Soc. London, Ser. A*, *335*, 243–259.

Kimura, G., et al. (1997), *Proceedings of the Ocean Drilling Program, Initial Reports*, vol. 170, Ocean Drill. Program, College Station, Tex.

Kimura, G., Y. Kitamura, Y. Hashimoto, A. Yamaguchi, T. Shibata, K. Ujiie, and S. Okamoto (2007), Transition of accretionary wedge structures around the up-dip limit of the seismogenic subduction zone, *Earth Planet. Sci. Lett.*, *255*, 471–484.

Kondo, H., G. Kimura, H. Masago, K. Ohmori-Ikehara, Y. Kitamura, E. Ikesawa, A. Sakaguchi, A. Yamaguchi, and S. Okamoto (2005), Deformation and fluid flow of a major out-of-sequence thrust located at seismogenic depth in an accretionary complex: Nobeoka Thrust in the Shimanto Belt, Kyushu, Japan, *Tectonics*, *24*, TC6008, doi:10.1029/2004TC001655.

Kübler, B., and M. Jaboyedoff (2000), Illite crystallinity, *Earth Planet. Sci. Lett.*, *331*, 75–89.

Kusaba, Y., A. Yamaguchi, G. Kimura, S. Okamoto, H. Yamaguchi, and T. Shibata (2006), The architecture of a fossilized out-of-sequence thrust in ancient accretionary complex: Footwall of the Nobeoka Thrust, Japan, *Eos Trans. AGU*, *87*(52), Fall Meet. Suppl., Abstract T21A-0375.

Kusky, T. M., and D. C. Bradley (1999), Kinematic analysis of melange fabrics: examples and applications from the McHugh Complex, Kenai Peninsula, Alaska, *J. Struct. Geol.*, *21*, 1773–1796.

Kusky, T. M., D. C. Bradley, P. J. Haeussler, S. Karl, and D. D. Thomas (1993), The Chugach Bay Thrust, a major tectonic boundary in the Southern Alaska accretionary prism, *Geol. Soc. Am. Abstr. Programs*, *25*(6), 282.

Kusky, T. M., D. C. Bradley, P. J. Haeussler, and S. Karl (1997), Controls on accretion of flysch and melange belts at convergent margins: Evidence from the Chugach Bay Thrust and Iceworm Melange, Chugach accretionary wedge, Alaska, *Tectonics*, *16*(6), 855–878.

Lay, T., et al. (2005), The Great Sumatra-Andaman earthquake of 26 December 2004, *Science*, *308*(5725), 1127–1133.

Magoon, L. B., W. L. Adkison, and R. M. Egbert (1976), Map showing geology, wildcat wells, Tertiary plant fossils, K-Ar age dates, and petroleum operations, Cook Inlet area, Alaska, scale 1:250,000, *U.S. Geol. Surv. Misc. Invest. Ser. Map*, I-1019.

McCann, T., and R. K. Pickerill (1988), Flysch trace fossils from the Cretaceous Kodiak Formation of Alaska, *J. Paleontol.*, *62*(3), 330–348.

Moore, G. W. (1969), New formations on Kodiak and adjacent islands, Alaska, *U.S. Geol. Surv. Bull.*, *1274-A*, A27–A35.

Moore, J. C. (1978), Orientation of underthrusting during latest Cretaceous and earliest Tertiary time, Kodiak Islands, Alaska, *Geology*, *6*(4), 209–213.

Moore, J. C., and A. Allwardt (1980), Progressive deformation of a Tertiary trench slope, Kodiak Islands, Alaska, *J. Geophys. Res.*, *85*(B9), 4741–4756.

Moore, J. C., and T. Byrne (1987), Thickening of fault zones: A mechanism of melange formation in accreting sediments, *Geology*, *15*, 1040–1043.

Moore, J. C., and R. L. Wheeler (1978), Structural fabric of a melange, Kodiak Islands, Alaska, *Am. J. Sci.*, *278*, 739–765.

Moore, J. C., T. Byrne, P. W. Plumley, M. Reid, H. Gibbons, and R. S. Coe (1983), Paleogene evolution of the Kodiak Islands, Alaska: Consequences of ridge-trench interaction in a more southerly latitude, *Tectonics*, *2*(3), 265–293.

Myers, G., and P. J. Vrolijk (1986), Fluid evolution associated with the accretion of the Kodiak Formation, Kodiak Island, Alaska, *Eos Trans. AGU*, *67*, 1219.

Ohmori, K., A. Taira, H. Tokuyama, A. Sakaguchi, M. Okamura, and A. Aihara (1997), Paleothermal structure of the Shimanto accretionary prism, Shikoku, Japan: Role of an out-of-sequence thrust, *Geology*, *25*(4), 327–330.

Okamoto, S., G. Kimura, S. Takizawa, and H. Yamaguchi (2006), Earthquake fault rock indicating a coupled lubrication mechanism, *eEarth*, *1*, 23–28, http://www.electronic-earth.net/1/23/2006/.

Orange, D. L., D. S. Geddes, and J. C. Moore (1993), Structural and fluid evolution of a young accretionary complex: The Hoh rock assemblage of the western Olympic Peninsula, Washington, *Geol. Soc. Am. Bull.*, *105*, 1053–1075.

Park, J.-O., T. Tsuru, S. Kodaira, A. Nakanishi, S. Miura, Y. Kaneda, Y. Kono, and N. Takahashi (2000), Out-of-sequence thrust faults developed in the coseismic slip zone of the 1946 Nankai earthquake (M_w = 8.2) off Shikoku, southwest Japan, *Geophys. Res. Lett.*, *27*(7), 1033–1036.

Paterson, S., and J. C. Sample (1988), The development of folds and cleavages in slate belts by underplating in accretionary complexes: A comparison of the Kodiak Formation, Alaska and the Calaveras Complex, California, *Tectonics*, *7*(4), 859–874.

Plafker, G. (1972), Alaskan Earthquake of 1964 and the Chilean Earthquake of 1960: Implications for Arc Tectonics, *J. Geophys. Res.*, *77*, 901–925.

Plafker, G., and W. Nokleberg (1987), Emplacement of accretionary assemblages of the Chugach Terrane, Alaska, *Geol. Soc. Am. Abstr. Programs*, *19*, 440.

Plafker, G., J. C. Moore, and G. R. Winkler (1994), Chapter 12: Geology of the southern Alaska margin, in *The Geology of North America*, vol. G-1, *The Geology of Alaska*, edited by G. Plafker and B. H. C., pp. 389–449, Geol. Soc. of Am., Boulder, Colo.

Rahn, M. K., and J. Mullis (2003), The influence of dolomite on illite crystallinity, *Geophys. Res. Abstr.*, *5*, 08642.

Riedel, M., G. D. Spence, N. R. Chapman, and R. D. Hyndman (2002), Seismic investigations of a vent field associated with gas hydrates, offshore Vancouver Island, *J. Geophys. Res.*, *107*(B9), 2200, doi:10.1029/2001JB000269.

Robinson, D., L. N. Warr, and R. E. Bevins (1990), The illite 'crystallinity' technique: A critical appraisal of its precision, *J. Metamorph. Geol.*, *8*, 333–344.

Roedder, E. (1984), *Fluid Inclusions*, *Rev. Mineral.*, vol. 12, BookCrafters, Chelsea, Mich.

Roeske, S. M. (1986), Field relations and metamorphism of the Raspberry Schist, Kodiak Islands, Alaska, in *Blueschists and Eclogites*, edited by B. W. Evans and E. H. Brown, *Spec. Pap. Geol. Soc. Am.*, *164*, 169–184.

Roeske, S. M., J. M. Mattison, and R. L. Armstrong (1989), Isotopic ages of glaucophane schists on the Kodiak Islands, southern Alaska, and their implications for the Mesozoic tectonic history of the Border Ranges fault system, *Geol. Soc. Am. Bull*, *101*, 1027–1037.

Rowe, C. D., E. Thompson, and J. C. Moore (2002), Contrasts in faulting and veining across the aseismic to seismic transition, Kodiak Accretionary Complex, Alaska, *Eos Trans. AGU*, *83*(47), Fall Meet. Suppl., Abstract T21A-1060.

Sakaguchi, A. (1999), Thermal maturity in the Shimanto accretionary prism, southwest Japan, with the thermal change of the subducting slab: Fluid inclusion and vitrinite reflectance study, *Earth Planet. Sci. Lett.*, *173*, 61–74.

Sample, J. C., and D. Fisher (1986), Duplex accretion and underplating in an ancient accretionary complex, Kodiak Islands, Alaska, *Geology*, *14*, 160–163.

Sample, J. C., and J. C. Moore (1987), Structural style and kinematics of an underplated slate belt, Kodiak and adjacent islands, Alaska, *Geol. Soc. Am. Bull.*, *86*, 1329–1336.

Sample, J. C., and M. R. Reid (2003), Large-scale, latest Cretaceous uplift along the Northeast Pacific Rim: Evidence from sediment volume, sandstone petrography, and Nd isotope signatures of the Kodiak Formation, Kodiak Islands, Alaska, in *Geology of a Transpressional Orogen Developed During Ridge-Trench Interaction Along the North Pacific Margin*, edited by V. B. Sisson, S. M. Roeske, and T. L. Pavlis, *Spec. Pap. Geol. Soc. Am.*, *371*, 51–70.

Shelton, K. L., M. B. Underwood, I. B. Burstein, G. T. Haeussler, and D. G. Howell (1996), Stable-isotope and fluid-inclusion studies of hydrothermal quartz and calcite veins from the Kandik thrust belt of east-central Alaska—Implications for thermotectonic history and terrane analysis, in *Thermal Evolution of Sedimentary Basins in Alaska*, edited by M. J. Johnsson and D. G. Howell, *U.S. Geol. Surv. Bull.*, *2142*, 111–131.

Silver, E. A., M. Kastner, A. Fisher, J. Morris, K. McIntosh, and D. Saffer (2000), Fluid flow paths in the Middle America Trench and Costa Rica margin, *Geology*, *28*(8), 679–682.

Sweeney, J. J., and A. K. Burnham (1990), Evaluation of a simple model of vitrinite reflectance based on chemical kinetics, *AAPG Bull.*, *74*(10), 1559–1570.

Taira, A., J. Katto, M. Tashiro, M. Okamura, and K. Kodama (1988), The Shimanto Belt in Shikoku, Japan: Evolution of Cretaceous to Miocene accretionary prism, *Mod. Geol.*, *12*(1–4), 5–46.

Thompson, E. (2002), Structural Analysis of the Ghost Rocks and Sitkalidak formations in the Kodiak Islands, Alaska, B.S. thesis, Univ. of Calif.

Torres, M. E., B. M. A. Teichert, A. M. Tréhu, W. Borowski, and H. Tomaru (2004), Relationship of pore water freshening to accretionary processes in the Cascadia margin: Fluid sources and gas hydrate abundance, *Geophys. Res. Lett.*, *31*, L22305, doi:10.1029/2004GL021219.

Tsuji, T., G. Kimura, S. Okamoto, F. Kono, H. Mochinaga, T. Saeki, and H. Tokuyama (2006), Modern and ancient seismogenic out-of-sequence thrusts in the Nankai accretionary prism: Comparison of laboratory-derived physical properties and seismic reflection data, *Geophys. Res. Lett.*, *33*, L18309, doi:10.1029/2006GL027025.

Underwood, M. B., and M. M. Laughland (2001), Paleothermal structure of the Point San Luis slab of central California: Effects of Late Cretaceous underplating, out-of-sequence thrusting, and late Cenozoic dextral offset, *Tectonics*, *20*(1), 97–111.

Underwood, M. B., J. P. Hibbard, and L. DiTullio (1993a), Geologic summary and conceptual framework for the study of thermal maturity within the Eocene-Miocene Shimanto Belt, Shikoku, Japan, in *Thermal Evolution of the Tertiary Shimanto Belt, Southwest Japan: An Example of Ridge-Trench Interaction*, edited by M. B. Underwood, *Spec. Pap. Geol. Soc. Am.*, *273*, 1–24.

Underwood, M. B., M. M. Laughland, and S. M. Kang (1993b), A comparison among organic and inorganic indicators of diagenesis and low-temperature metamorphism, Tertiary Shimanto Belt, Shikoku, Japan, in *Thermal Evolution of the Tertiary Shimanto Belt, Southwest Japan: An Example of Ridge-Trench Interaction*, edited by M. B. Underwood, *Spec. Pap. Geol. Soc. Am.*, *273*, 45–61.

Underwood, M. B., D. G. Howell, M. J. Johnsson, and M. J. Pawlewicz (1996), Thermotectonic evolution of suspect terranes in the Kandik region of east-central Alaska, in *Thermal Evolution of Sedimentary Basins in Alaska*, edited by M. J. Johnsson and D. G. Howell, *U.S. Geol. Surv. Bull.*, *2142*, 81–110.

Vrolijk, P. (1987a), Paleohydrogeology and fluid evolution of the Kodiak accretionary complex, Alaska, Ph.D. thesis, Univ. of Calif., Santa Cruz.

Vrolijk, P. (1987b), Tectonically driven fluid flow in the Kodiak accretionary complex, Alaska, *Geology*, *15*, 466–469.

Vrolijk, P., and B. A. van der Pluijm (1999), Clay gouge, *J. Struct. Geol.*, *21*, 1039–1048.

Vrolijk, P., G. Myers, and J. C. Moore (1988), Warm fluid migration along tectonic melanges in the Kodiak Accretionary Complex, Alaska, *J. Geophys. Res.*, *93*(B9), 10,313–10,324.

Vrolijk, P. J. (1985), Fluid and paleohydrologeologic evolution during progressive melange deformation, *Geol. Soc. Am. Abstr. Programs*, *17*(6), 415.

Wang, H., and J. Zhou (2000), The relationships between the Kübler index, Weaver index and Weber index of illite crystallinity and their applications, *Schweiz. Mineral. Petrogr. Mitt.*, *80*, 187–198.

Zwart, G., J. C. Moore, and G. R. Cochrane (1996), Variations in temperature gradients identify active faults in the Oregon accretionary prism, *Earth Planet. Sci. Lett.*, *139*(3–4), 485–495.

F. Meneghini, Dipartimento di Scienze della Terra, Universitá di Pisa, via Santa Maria, 53, Pisa, I-56126 Italy.

J. C. Moore, Earth and Planetary Sciences, University of California, Santa Cruz, 1156 High Street, Santa Cruz, CA 95060, USA.

C. D. Rowe, Department of Geological Sciences, University of Cape Town, Private Bag X3, Rondebosch, 7701 South Africa. (christie.rowe@uct.ac.za)